DEPARTMENT OF THE INTERIOR
U.S. GEOLOGICAL SURVEY

Red-Sea rift magmatism near Al Lith, Kingdom of Saudi Arabia

by

John S. Pallister[1/]

Open-File Report 86-565

Report prepared by the U.S. Geological Survey in cooperation with the Deputy Ministry for Mineral Resources, Saudi Arabia

This report is preliminary and has not been reviewed for conformity with U.S. Geological Survey editorial standards and stratigraphic nomenclature.

1/ USGS Denver, CO

1986

TABLE OF CONTENTS

ILLUSTRATIONS

PAGE

TABLES

RED-SEA RIFT MAGMATISM NEAR AL LITH, KINGDOM OF SAUDI ARABIA

BY

JOHN S. PALLISTER 1/

ABSTRACT

A newly recognized Tertiary dike complex and comagmatic volcanic rocks exposed on the central Saudi Arabian coastal plain record early stages of magmatism related to Red Sea rifting. Intrusive and stratigraphic relationships, and new potassium-argon dating indicate episodic magmatism from about 30 Ma to the present. Additional stratigraphic and radiometric evidence suggests that limited rift-related magmatism may have began as early as about 50 Ma ago. An early phase of crustal extension in the region was accompanied by faulting and graben formation and by dike-swarm intrusion. The style of extension and intrusion changed approximately 20 Ma ago. Localized volcanism and sheeted dike injection ceased and were replaced by the intrusion of thick gabbro dikes. This change may mark the onset of sea-floor spreading in the central Red Sea.

The dikes and volcanic rocks consist of a bimodal mafic-felsic suite with transitional subalkaline to alkaline chemistry. Although no unique petrogenetic model can be developed for the suite, the following observations and conclusions are apparent from the available reconnaissance geochemistry: 1) Strontium isotopic initial ratios overlap in the range 0.7031 to 0.7047 and are not clearly related to alkalinity or silica content. Therefore, the bimodality and alkalinity of the suite are not products of contamination by the radiogenic Precambrian upper-crustal granitic rocks exposed in the region. 2) Several of the evolved rocks (rhyolites and comendite) show large to extreme negative europium anomalies and heavy rare-earth element (HREE) enrichment, features that cannot be explained by low-pressure crystal fractionation of potential parent magmas. An intriguing possibility is that HREE enrichments and large negative Eu anomalies of some peraluminous rhyolites (and granites) may result from the complete melting of garnet from middle or lower crustal rocks. 3) Most of the basalts are light rare-earth element (LREE)-enriched, consistent with derivation from fertile mantle in a continental-rift setting, however, interaction of the mafic melts with lower continental crust cannot be ruled out.

A model of poly-baric mantle-melt derivation, producing several alkaline-subalkaline cycles, best explains magmatism in the Red Sea region. Differences in the depths and dynamics of mantle-melt extraction and transport brought about through changes in crust and mantle structure as the rift and paar developed may account for the transition from mixed alkaline-subalkaline bimodal magmatism of the pre-20 Ma rift basin to exclusively subalkaline (tholeiitic) magmatism at the Red Sea spreading axis and to predominantly alkali basalt volcanism within the Arabian Shield.

1/ USGS, Denver, CO

INTRODUCTION

RELEVANCE OF THIS STUDY

The Red Sea is a young (principally <20 Ma) basin that is floored (in part) by ocean crust and that developed by rifting of the Arabian-Nubian Precambrian Shield during the Tertiary (Schmidt and others, 1982; Cochran, 1983; Coleman, 1984a; Bohannon, 1986, unpub. data). The basin and flanking areas provide insight into tectonic and magmatic processes that accompany continental rifting and the transition from continental to oceanic volcanism. Igneous rocks related in space and time to formation of the Red Sea are exposed near the Afar triple junction in East Africa and Yemen, in the East African rift zones, on the coastal plain and in the axial deep of the Red Sea, and as flood basalt fields bordering the Red Sea. Each of these geographic areas contain rocks that were produced during different phases of rifting and sea-floor spreading (Coleman, 1974; 1984a). Axial areas of the Red Sea record only the most recent (<5 Ma) spreading history and the production of tholeiitic basalt similar to MORB; the Red Sea shelves are blanketed by thick evaporites and clastic and biogenic sediments that are underlain by oceanic, transitional, and continental crust (Cochran, 1983; Blank and others, 1986). The flood basalt fields consist mainly of alkali olivine basalt produced during the period of rifting and sea-floor spreading, but erupted along fissures east of the principal zone of extension and mainly in Saudi Arabia, Yemen, and Jordan (Coleman and others, 1983; Coleman, 1984a). The coastal plain is unusual in having exposures of rocks that record the earliest stages of rifting, as well as the transition from continental to proto-oceanic crust (Gettings, 1977; Schmidt and others, 1982; Blank and others, 1986).

This study focuses on the record of rift-related magmatism in a region of the central Saudi Arabian coastal plain. Geologic mapping in the area (Pallister, 1986) led to the discovery of rift-related dike swarms and small plutons that are cogenetic with isolated exposures of volcanic rocks and that provide new age constraints and chemical characteristics for initial Red Sea rift magmatism. The style of intrusion in the area is related to tectonic changes during rifting. The chemistry of the magmas produced during rifting show a transition from continental to oceanic domains, a transition that characterizes the initial stages of ocean basin formation.

PREVIOUS INVESTIGATIONS IN THE AL LITH AREA

This report is based on geologic mapping of the Al Lith 1° X $1^{o}30'$ quadrangle (Pallister, 1986), which lies in the coastal plain-piedmont province of west-central Saudi Arabia about 80 kilometers southeast of Jeddah (fig. 1). Details of the Precambrian geology of the region are presented by Pallister (1986); this report is concerned only with the record of Red Sea rifting preserved in rocks of mostly Tertiary age within the quadrangle. Except for the Wajid Sandstone, all rock unit names used in this report are informal and capitalization follows Saudi Arabian stratigraphic nomenclature (Fitch, 1980).

Previous geologic mapping in the Al Lith region includes the work of Brown and others (1963), Wier and Hadley (1975), Hadley and Fleck (1980), and Pallister (1982a + b, unpub. data; 1982c). Geophysical data for the quadrangle were compiled from a regional report by ARGAS (1977) and from an airborne magnetometer survey (Riofinex, 1980). Gravity data for part of the area have recently been compiled by M. E. Gettings (Gettings, 1983, 1984; Gettings and others, 1983).

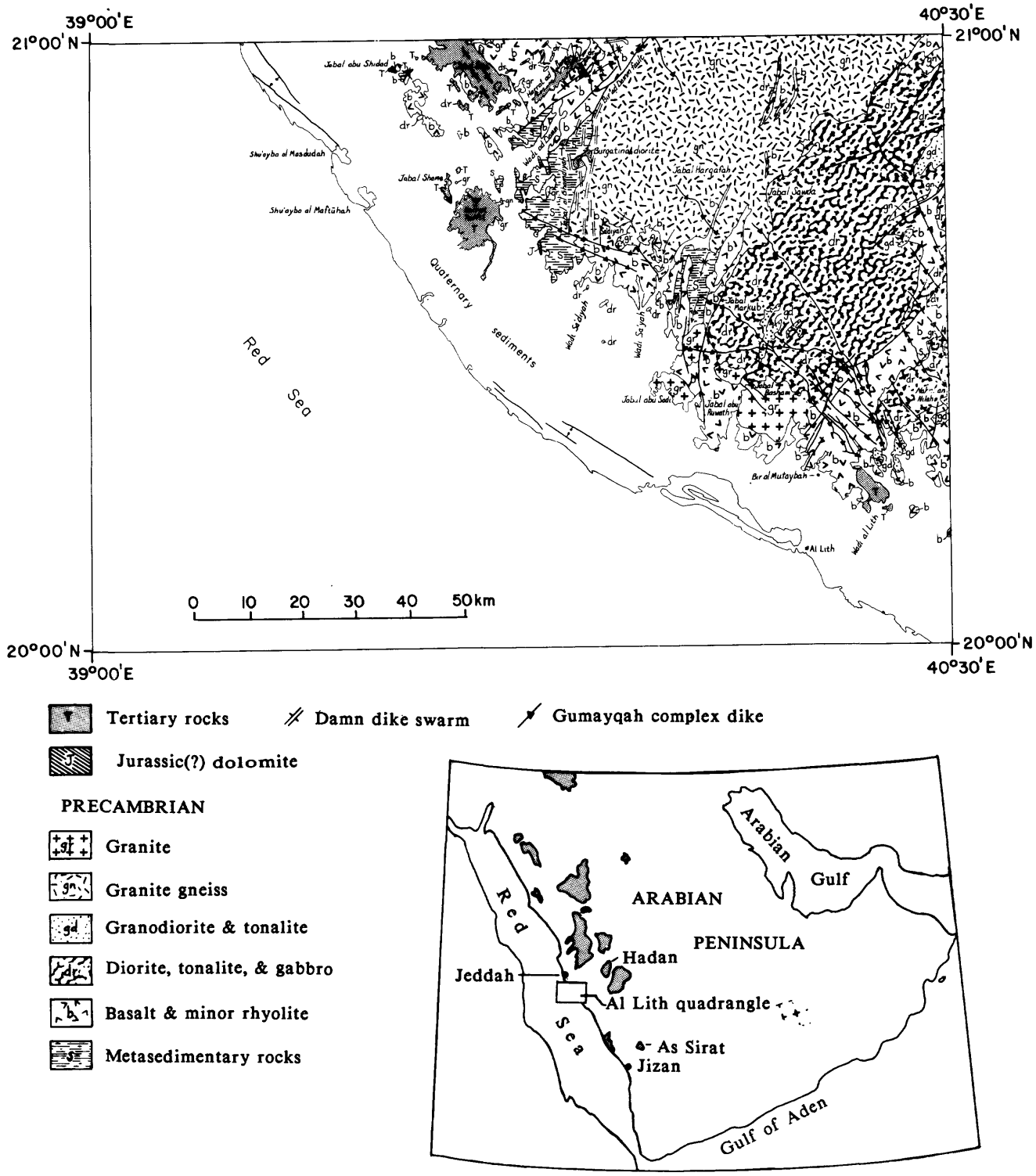

Figure 1.--*Simplified geologic map of the Al Lith quadrangle; index map of the Arabian Peninsula shows location of the quadrangle, and distribution of Tertiary-Quaternary alkali flood-basalt fields (shaded areas).*

GEOLOGIC AND TECTONIC SETTING

The Precambrian Arabian Shield was eroded to a peneplain prior to deposition of Paleozoic and Mesozoic sedimentary rocks (Powers and others, 1966). The western Arabian Shield remained a stable platform throughout the Paleozoic and Mesozoic; deformation and magmatism associated with Red Sea rifting represent the only major orogenic event to affect the region since the close of the Precambrian.

Continental rifting related to formation of the Red Sea took place mostly during the middle Tertiary (Schmidt and others, 1982). The interior (Najd) plateau was uplifted during the Miocene and Pliocene, forming the Red Sea escarpment. Eruption of alkali olivine flood basalts, known as Harrat (plateau) basalts, in western Arabia began about 30 Ma ago and has continued virtually to the present (Coleman and others, 1983).

Late Proterozoic plutonic, meta-volcanic, and meta-sedimentary rocks are exposed throughout most of the Al Lith region. Tertiary sedimentary, volcanic, and plutonic rocks are exposed in and near the coastal plain, and Tertiary oceanic crust of the Red Sea is inferred to exist beneath the outer coastal plain and offshore (fig. 1). The contact between oceanic (or transitional in the sense of Gettings and others, 1983; and Blank and others, 1986) and continental crust is marked by a steep gravity gradient and magnetic lineament, located 10-15 kilometers onshore (fig. 1 and Pallister, 1986). The Tertiary igneous rocks described in this report are exposed east of the contact and intrude extended Proterozoic continental crust. The coastal plain is blanketed by Quaternary sediments and fringed by coral reefs.

TERTIARY ROCKS

The distribution of Tertiary rocks in the region and place names used in the text are shown in Figures 1 and 2. The physical features and petrography of the rocks in the Al Lith quadrangle are described by Pallister (1986). Characteristics of Tertiary rock units and relationships to rift processes are summarized below. Potassium-argon and fission-track dates that are cited in the following rock-unit descriptions are listed in table 1.

The three Tertiary rock units of principal concern to this report are the Sita formation and the Damm and Gumayqah intrusive complexes. The Sita is a mostly volcanic and volcaniclastic unit that is cogenetic with dike rocks that comprise the Damm complex. The Gumayqah complex consists of thick dikes that postdate the Sita and Damm rocks. Other Tertiary rock units in the region that are described below provide stratigraphic or intrusive relations that constrain the timing and character of rift magmatism.

Volcanic rock names are assigned using the chemical classification system of Irvine and Baragar (1971). It should be emphasized that the Al Lith rocks are transitional from alkaline (sodic series) to subalkaline in character, therefore, strict application of chemical classification leads to ambiguous and somewhat artificial results in borderline cases. However, the mafic rocks range from nepheline-normative alkali basalt to hypersthene- and quartz-normative tholeiite. There is also petrographic evidence of alkaline and subalkaline compositions:

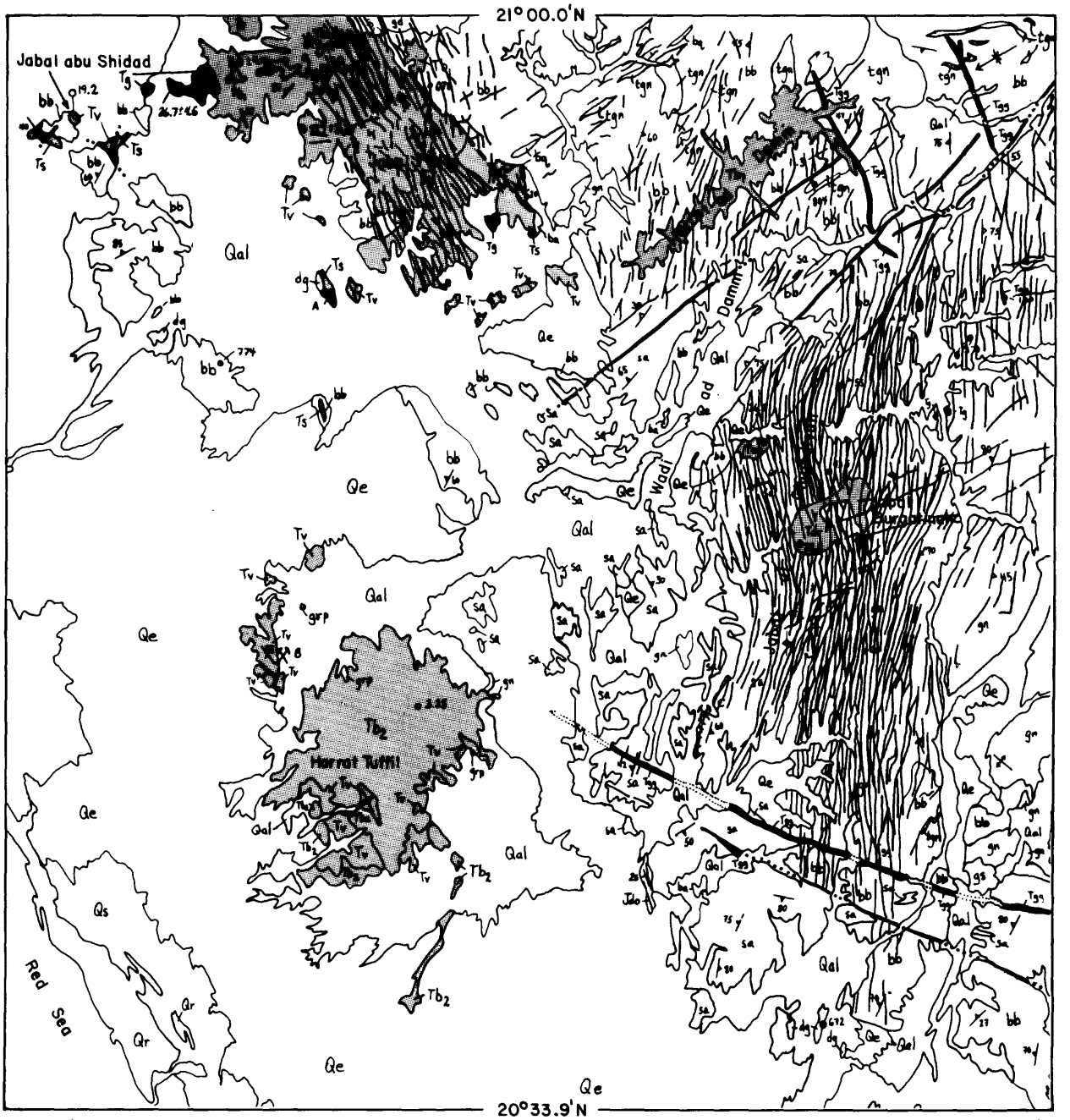

Qe	-	Eolian deposits	Tan	-	Anorthosite	PRECAMBRIAN ROCKS				K-Ar DATES (±1 given if >5%)	
Qal	-	Alluvian deposits	Tdr	-	Burgatinah diorite	gs	-	Syenogranite		o- 26.0±4.5 - whole rock sample	
Qr	-	Reef limestone	Tg	-	Gabbro	grp	-	Peraluminous granite		o- 804 - Mineral separate	
Qs	-	Sabkah deposits	Td	-	Dam dike complex	gn	-	Granite gneiss		⚒ - MINERAL PROSPECT	
Tb_2	-	Pilocene alkali basalt	Tv	-	Sita formation	dg	-	Diorite and gabbro		- Prominent dikes	
Tba	-	Batham formation	Ts	-	Shumaysi formation	tgn	-	Tonalite gneiss			
Tb_1	-	Miocene alkali basalt	Jdo	-	Dolomite	bb	-	Metasalt			
Tgg	-	Gumayqah complex				sa	-	Metasediments			

Figure 2.--*Simplified geologic map showing prominent dikes of the Damm and Gumayqah complexes and Tertiary gabbro stocks (screened). Other Tertiary rocks are shaded.*

TABLE 1.--K-Ar age data for rocks from the Al Lith region

[K-Ar dates calculated (or recalculated) using constants recommended by Steiger and Jäger (1977): ^{40}K = 0.01167 atom %, λ_β = 4.962 X $10^{-10}y^{-1}$, λ_ε = 0.5811 X $10^{-10}y^{-1}$. K and Ar abundance data only given for samples analyzed during this study. References: A= Brown, 1970; data shown in Gettings and Stoeser (1981), B= Brown, unpublished data shown in Gettings and Stoeser, 1981, C= Marvin, unpublished data shown in Gettings and Stoeser (1981). K-Ar determinations by Australian Mineral Development Laboratories (AMDEL)*, Frewville, South Australia.]

Unit Symbol	Latitude North	Longitude East	Sample number	Rock type	Material analyzed	%K	$^{40}Ar_r$ (X 10^{-10} mol/g)	$\frac{^{40}Ar_r}{^{40}Ar_t}$	Date (Ma)	±1σ	Reference
Tv	20°54'	39°38.5'	66	Trachyte	Whole rock				21.1	±2.2	A
Tb_2	20°44'	39°41'	5MX68	Basalt	Whole rock				3.0	±0.2	A
Tb_2	20°44'	39°41'	165006	Basalt	Whole rock	1.157	0.06536	0.470	3.25	±0.05	This paper
						1.156					
Tb_1	20°57'	39°35'	6MX68	Basalt	Whole rock				7.0	±4.4	A
Tb_1	20°56'	39°52'	165568	Basalt	Clinopyroxene	0.012	0.00237	0.028	11.3	±0.6	This paper
						0.012					
Tv	20°56'	39°31'	926	Rhyolite	Whole rock				19.2	±0.9	B
Tg	20°59'	39°38'	927A	Gabbro(pluton)	Whole rock				26.7	±4.6	B
Tg	20°59'	39°38'	927B	Gabbro(pluton)	Whole rock				27.9	±5.6	B
Tgg	20°24'	40°21.5'	928A	Gabbro(dike)	Whole rock				18.0	±3.1	B
Tgg	20°24'	40°21.5'	928B	Gabbro(dike)	Whole rock				25.2	±1.8	B
Tgg	20°24'	40°21.5'	928C	Gabbro(dike)	Whole rock				23.3	±1.3	B
Tgg	20°24'	40°21.5'	928D	Gabbro(dike)	Whole rock				20.7	±1.2	B
Tgg	20°26.5'	40°13'	623A	Gabbro(dike)	Whole rock				179	±12	C
Tgg	20°53'	39°55'	165634	Gabbro(dike)	Whole rock	0.153	0.36015	0.539	131	±2	This paper
						0.153	0.35372	0.533	129	±2	
Tgg	20°28.0'	40°12.2'	175764	Gabbro(dike)	Plagioclase	0.247	0.09343	0.299	21.7	±0.5	This paper
						0.246					
Tgg	20°28.0'	40°12.2'	175764	Gabbro(dike)	Clinopyroxene	0.024	0.01020	0.044	24.4	±1.2	This paper
						0.024					
Td	20°49.0'	39°51.9'	165559	Hawaiite(dike)	Plagioclase	0.608	0.46495	0.504	43.5	±0.7	This paper
						0.611					
Tan	20°50'	39°50'	165614	Leucogabbro	Hornblende	1.085	0.50217	0.653	26.5	±0.4	This paper
						1.084					
Tdr	20°47.7'	39°51.2'	165570	Quartz diorite	Hornblende	0.772	0.36201	0.602	26.8	±0.4	This paper
						0.771					
Tdr	20°47.7'	39°51.3'	165574	Quartz diorite	Hornblende	0.532	0.25931	0.512	27.8	±0.4	This paper
						0.533					
Tdr	20°47.7'	39°51.4'	165865	Monzonite	Hornblende	0.521	0.24794	0.584	27.2	±0.4	This paper
						0.521					
Tv	20°17'	40°20'	175711	Basalt(sill?)	Plagioclase	0.168	0.2546	0 589	85.6	±1 7	This paper
						0.167					
Tv	20°17'	40°20'	175711	Basalt(sill?)	Clinopyroxene	0.0077	0.02226	0.188	158	±8	This paper

*Use of company names is for descriptive purposes only and does not imply endorsement by the U.S. Geological Survey.
Unit symbols defined in Figure 2 and in text.

groundmass olivine is common in the alkali basalts, but is lacking in the tholeiites, Coleman and others (1983) report groundmass nepheline in the Harrat basalts, and Al Lith area felsic rocks range from quartz-phyric rhyolite to fayalite-, aegirine-, and arfvedsonite-bearing trachyte and comendite (Pallister, 1986). Dispite the ambiguity for transitional rocks, and because of the need to describe a relatively diverse suite of volcanic and hypabyssal rocks, a rigorous chemical classification scheme is employed.

MUTAYBAH LATERITE

A single strike-ridge of pisolitic, ferruginous laterite unconformably overlies Proterozoic rocks east of Bir al Mutaybah (fig. 1). The laterite is 2-3 meters thick and is overlain by a poorly exposed 30-40 meter thick section of volcanic and volcaniclastic rocks of the Sita formation. The laterite is one of the youngest rock unit that is clearly overlain by the Sita formation and therefore provides a maximum stratigraphic age for rift volcanism in the region.

A number of laterite occurrences are reported from the upper Cretaceous and Paleogene of the Red Sea region (see review by Moltzer and Binda, 1981), therefore, more than one stratigraphic correlation is possible. Schmidt and others (1982) correlate the Mutaybah laterite with early Tertiary laterites exposed below the As Sirat and Harrat Hadan basalt fields (fig. 1) based on lithologic similarity and geologic setting of the deposits (overlying Proterozoic rocks and underlying late Oligocene-early Miocene basalts). At Harrat Hadan ferruginous and pisolitic laterite overlies the Paleocene Umm Himar formation and underlies basalt flows of about 28 Ma (Madden and others, 1979). The Paleocene age of the Umm Himar is based on paleontologic data (Madden and others, 1979; Madden, 1983). Also at Harrat Hadan, a ferruginous and oolitic mudstone forms the base of the Umm Himar formation and unconformably overlies either the Cretaceous Khurma formation or Precambrian basement (Madden and others, 1979). Therefore, correlation with laterite near Harrat Hadan would bracket the Mutaybah and earliest rift volcanism between the Cretaceous (and possibly the Paleocene) and about 28 Ma.

SHUMAYSI FORMATION

The name Shumaysi formation (Karpoff, 1957a, b) was used by Brown and others (1963) and Al-Shanti (1966) for a sequence of east-dipping north-northwest-trending homoclinal ridges of sandstone, siltstone, and oolitic ironstone exposed near the village of Ash Shumaysi (50 kilometers north of the Al Lith quadrangle). The formation can be traced discontinuously south from the type area to isolated, commonly fault-bounded exposures near Jabal Sita and Jabal abu Shidad in the northern part of the Al Lith quadrangle.

The formation in the Jabal Sita-Jabal abu Shidad area is composed of quartz arenite, hematitic quartz arenite, hematitic claystone, and ironstone. The Shumaysi unconformably overlies Proterozoic rocks and regionally underlies, but is locally interbedded with, tuffaceous rocks of the Sita formation (Pallister, 1982c, 1986). Contacts with the underlying Proterozoic rocks and overlying Sita formation are typically faults; however, east of Jabal Sita hematitic-matrix Shumaysi sandstone overlies Proterozoic metabasalt and southwest of Jabal Sita the sandstone contains interbedded Sita water-lain tuff beds.

The quartz arenitic composition, strained quartz grains, and trace heavy-mineral assemblage indicate that the Shumaysi formation was derived from Precambrian granitic and metamorphic rocks (Pallister, 1986). Abundant hematite and ironstone beds suggest that iron was derived from subtropical(?), deeply weathered, lateritic soils developed on the Precambrian surface. Moltzer and Binda (1981) suggest a terrestrial depositional environment similar to Lake Chad for the middle member of the Shumaysi on the basis of the abundance and variety of pollen and spores and the presence of leaf remains, wood fragments, and interbeds of oolitic ironstone. The fossil assemblage of the upper member suggests a change in depositional environment to "in or near an estuary that opened into a shallow sea" (Moltzer and Binda, 1981).

The Shumaysi is intruded by sparse basalt and plagioclase-megacryst bearing hawaiite dikes of the Damm dike complex southeast of Jabal Sita. This intrusive relation and interbedding with tuffaceous rocks of the Sita formation indicate that although most of the Shumaysi probably predates the Sita formation, at least the latest members of the Shumaysi were being deposited during early Sita volcanism and related Damm-dike-complex intrusion. A volcanic ash bed was also mapped within the upper member of the Shumaysi formation in the type area by Al-Shanti (1966).

Fossil assemblages from samples of the middle member of the Shumaysi formation define an early Eocene (Cusian) age (Moltzer and Binda, 1981). The age of the upper member of the Shumaysi is debated. It has been assigned both Eocene and Oligocene ages (see Al-Shanti, 1966). Moltzner and Binda (1981) concluded on the basis of the early Eocene age of the middle member, the intervening sediment thickness (about 60 meters), and the high rates of sedimentation that prevail in estuarine environments that an Eocene age for the upper member is more reasonable than an Oligocene age. However, D. L. Schmidt (written commun. 1985) considers the upper Shumaysi of the Al Lith region to probably be Oligocene on the basis of possible correlation with the Ayyanah sandstone of the southern coastal plain.

SITA FORMATION

The Sita formation was defined by Pallister (1982c, 1986) for the Tertiary volcanic, volcaniclastic, and associated sedimentary rocks exposed chiefly in the vicinity of Jabal Sita. The volcanic members of the formation comprise a bimodal mafic-felsic suite with transitional subalkaline to alkaline chemistry. Principal rock types are: alkali basalt, hawaiite, trachyte, and subalkaline basalt, dacite, and rhyolite. Near Jabal Sita, the volcanic rocks form lava flows that are interbedded with volcaniclastic rocks (tuff breccia and water-lain tuff), graywacke, laminated (lacustrine?) limestone, and shale. An overall stratigraphic or time progression from alkaline to subalkaline compositions (or vice versa) is not apparent from reconnaissance mapping.

A rhyolite plug intrudes Precambrian metabasalt at Jabal abu Shidad, and nearby Sita lava flows unconformably overlie Precambrian metabasalt. The Sita formation is unconformably overlain by the Bathan formation, Pliocene alkali basalt at Harrat Tuffil, and Miocene alkali basalt north and northwest of Jabal Sita. The formation is intruded by subvertical, locally sheeted, north-to northwest-trending trachyte and sparse comendite dikes and by hawaiite or alkali basalt dikes of the Damm dike complex. The exposed thickness of the formation

is variable, but locally exceeds 300 meters (Pallister, 1982c); the upper contact is erosional.

Rhyolite from Jabal abu Shidad was dated by whole-rock K-Ar at 19.2±0.9 Ma and trachyte from near Jabal Sita was dated at 21.1±2.2 Ma (table 1). Zircon from perlitic rhyolite of a lava flow at Jabal Shama yielded a fission track date of 20.3±3.6 Ma (table 1). The lowest part of the Sita formation has not been unequivocally dated. However, the formation is probably cogenetic and coeval with the Damm dike complex (next section). Intrusive and stratigraphic relations and K-Ar dating indicate that the Sita and Damm rocks range in age from more than 27 Ma (and perhaps as old as about 50 Ma - early Eocene) to about 20 Ma.

DAMM DIKE COMPLEX

The Damm dike complex consists of two dense swarms of subparallel to parallel dikes and minor sills in the Jabal al Ghamdiyah and Jabal Sita regions (figs. 2 and 3). The complex was named after Wadi ad Damm by Pallister (1982c).

The dike complex contains a bimodal mafic-felsic suite of transitional alkaline to subalkaline chemistry: alkali basalt, hawaiite, trachyte, sparse comendite, and tholeiitic basalt, dacite, and rhyolite. This bimodal assemblage is very similar to the distribution of rock types in the Sita formation and the dike complex is regarded as the feeder zone for Sita volcanic rocks.

The dikes are variably altered and metamorphosed to greenschist facies without appreciable deformation. Dike chill-margins are easily recognized, and dikes average 1-2 meters in thickness. Dikes become more abundant inward from the margins of the swarms and form local zones of sheeted dike complex (100-percent dike rock). The dikes are typically parallel to subparallel and vertical to subvertical. Split dikes, formed by repeated parallel intrusion, are common locally. Sparse, cross-cutting dikes occur within the swarm and tend to follow northeast-trending regional basement structure. Mafic and felsic dikes (of both alkaline and subalkaline chemistry) intrude one another and consequently overlap in relative age.

Most dikes were intruded either in a north-trending swarm that follows the western boundary of a Precambrian granite gneiss batholith through Jabal al Ghamdiyah or in a separate, northwest-trending swarm in the Jabal Sita area (fig. 2). The dike complex is overlain unconformably by Miocene alkali basalt of Harrat ad Damm, dated at 11.3±0.6 Ma, and is intruded by large, west-northwest trending dikes (of the Gumayqah complex) east of Harrat Tuffil, dated at 21.7±5 Ma and at 24.4±1.2 Ma north of Jabal Basham (table 1). Alteration of the Damm complex dikes precludes direct radiometric dating in most cases, but, mineral separates from two dikes of the Jabal al Ghamdiyah swarm have been dated. Zircon from a dacite dike yielded a fission-track age of 23.2±3.2 Ma and fresh plagioclase megacrysts from a hawaiite dike gave a K-Ar date of 43.5±0.7 Ma.

Intrusive relations show that many of the dikes are older than 27 Ma. Most of the dikes within the Jabal al Ghamdiyah swarm are intruded by the Burgatinah diorite, which is dated at 26.8±0.4, 27.8±0.4, and 27.2±0.4 Ma. Hawaiite, tholeiite, and dacite to rhyolite dikes are intruded by the diorite. The remainder of the swarm (also containing tholeiite, hawaiite, and dacite dikes) intrudes the diorite. The dikes are truncated along a sharp intrusive boundary; inclusions of the dike rocks are observed within the diorite close to the contact.

Figure 3.--*Aerial view to northwest of Damm dike complex in Jabal al Ghamdiyah. Apparent north-south layering is produced by parallel, subvertical dikes that make up more than 50 percent of the outcrops in this area.*

The Shumaysi formation is intruded by sparse plagioclase megacryst bearing dikes southeast of Jabal Sita. The small number of dikes in the Shumaysi relative to the high concentration of dikes in nearby exposures of Proterozoic basement where the Shumaysi is stripped away indicates that either many of the dikes abruptly terminate below the Shumaysi, or that the Shumaysi unconformably overlies some dikes of the Damm complex. The latter would also be expected from the volcanic (tuffaceous) component in the Shumaysi, which implies magmatism during Shumaysi deposition. The intrusive relationships, coupled with stratigraphic and radiometric data from the cogenetic Sita formation, suggest that the dike complex was intruded over a period that began during Shumaysi deposition and continued until about 20 Ma ago.

If the age of the upper member of the Shumaysi is Eocene, as favored by Moltzer and Binda (1981), a prolonged interval of magmatism (from about 50 Ma to 20 Ma) would be indicated for the region. The 43.5±0.7 Ma hawaiite plagioclase date (table 1) is the central part of the Jabal al Ghamdiyah dike complex is the oldest radiometric date within this interval, and is thought to represent a magmatic age. However, some of the Tertiary hypabyssal rocks of Saudi Arabia are contaminated with excess argon (table 1), hence one must be skeptical of relatively old K-Ar age determinations on these rocks.

GABBRO

Two plutons of Tertiary gabbro crop out near Jabal Sita and are composed of medium- to coarse-grained, nonlayered, olivine-clinopyroxene gabbro. The rocks are generally fresh, except for limited alteration of olivine to smectite and serpentine. Pyroxene, plagioclase, and biotite have also undergone limited alteration to uralite, saussurite, and chlorite, respectively. The gabbro pluton west of Jabal Sita is dated by whole-rock K-Ar at 26.7±4.6 and 27.9±5.6Ma (table 1).

BURGATINAH DIORITE

A small (2- by 4-kilometers) pluton at Jabal Burgatinah is composed of quartz diorite, diorite, and monzodiorite. The pluton intrudes most dikes of the Damm complex (fig. 2 and 4). The rock is chemically subalkaline, the plutonic equivalent of dacite to andesite (table 2). As previously described, intrusive relations indicate that most dikes of the Damm complex predate the diorite but dike intrusion continued after emplacement of the pluton. The Burgatinah diorite is dated by hornblende K-Ar at 26.8±0.4, 27.8±0.4, and 27.2±0.4 Ma (table 1).

ANORTHOSITE AND LEUCOGABBRO

A small (1-kilometer diameter) pluton about 5 kilometers northwest of Jabal Burgatinah is composed of medium- to coarse-grained, hypidiomorphic granular biotite-, clinopyroxene-, and hornblende-bearing anorthosite and plagioclase-rich diorite and leucogabbro. The pluton intrudes most dikes of the adjacent Damm dike swarm, but it is intruded by sparse mafic dikes. Consequently, it is coeval with the late phase of Damm dike complex intrusion. The pluton, dated by hornblende K-Ar at 26.5±0.4 Ma (table 1), produces a prominent, normally polarized aeromagnetic anomaly similar to that of the Burgatinah diorite. It probably was intruded at the same time as, and is cogenetic with, the diorite.

Figure 4.--*Aerial view to northwest of the Tertiary Burgatinah diorite. The pluton margin is outlined by the circular valley in the middle ground; the pluton is approximately 2 kilometers across.*

TABLE 2.--Major element chemical analyses of rocks from the Al Lith region

[CIPW normative minerals calculated on a volatile-free basis and after adjustment of Fe_2O_3 and FeO following the procedure of Irvine and Baragar (1971). Analyses by X-ray flourescence, except FeO by wet chemistry (and Fe_2O_3 by difference from XRF value) and U and Th by instrumental neutron-activation analysis. Analyses performed by X-ray Assay Laboratories, Don Mills, Ontario, Canada, except U and Th for samples: 165006, 165531, 165546, 165574, 165661, 165714, and 165882 by USGS, Denver, Colorado, USA. Values are listed in weight percent, except where noted as parts per million (ppm). Volcanic rock names are based on the chemical classification method of Irvine and Baragar. "Alk.basalt" indicates alkali basalt of the sodic series of the alkali olivine basalt series of Irvine and Baragar (1971). "Basalt" indicates basalt of the tholeiitic basalt series of Irvine and Baragar. Coordinates from base maps used by Pallister (1982c) and Hadley and Fleck (1980). Use of company names is for descriptive purposes only and dose not imply endorsement by the U.S. Geological Survey.]

Sample No.	165006	165006	165582	165666	165667	165563	165593	165634	175764	175776
Unit symbol	Tb_2	Tb_2	Tb_1	Tb_1	Tb_1	Tgg	Tgg	Tgg	Tgg	Tgg
Rock type	Hawaiite	Hawaiite	Alk.basalt	Alk.basalt	Hawaiite	Gabbro (Basalt)	Basalt	Gabbro (Alk.basalt)	Gabbro (Basalt)	Diabase (Basalt)
N. Latitude	20°43.6'	20°43.6'	20°56.4'	20°59.2'	20°59.2'	20°48.9'	20°41.7'	20°53.3'	20°28.0'	19°23'
E. Longitude	39°41.5'	39°41.5'	39°52.4'	39°39.1'	39°39.1'	39°59.5'	39°46.5'	39°56.5'	40°12.2'	41°15'
SiO_2	47.1	48.1	46.3	44.6	45.5	52.9	47.3	47.1	50.2	46.9
Al_2O_3	17.0	17.0	15.3	15.8	16.0	16.6	14.5	16.3	18.2	13.8
Fe_2O_3	5.8	5.4	3.8	3.1	3.1	4.2	2.6	1.6	2.8	3.9
FeO	3.6	4.1	6.8	6.6	6.4	5.2	10.0	7.0	8.1	9.7
MgO	5.06	5.19	7.77	8.83	8.01	3.03	6.62	10.5	2.19	6.16
CaO	9.50	9.45	10.3	9.10	9.95	8.22	10.6	12.2	9.96	10.0
Na_2O	4.21	4.13	3.42	3.36	3.65	3.20	2.60	2.22	3.40	2.89
K_2O	1.37	1.51	0.78	1.12	1.10	1.42	0.46	0.17	0.89	0.48
LOI	1.08	0.39	0.70	2.00	1.00	1.77	<0.01	0.23	0.47	1.77
TiO_2	2.31	2.43	1.83	2.30	2.24	2.11	2.14	0.52	1.78	2.57
P_2O_5	0.58	0.58	0.35	0.47	0.48	0.24	0.25	0.06	0.51	0.33
MnO	0.16	0.15	0.16	0.16	0.16	0.14	0.20	0.15	0.18	0.21
Total	97.8	98.6	97.6	97.5	97.7	99.0	97.4	98.1	98.7	98.7
Cr(ppm)	120	100	280	180	200	70	120	520	30	70
Zr(ppm)	230	230	160	190	170	200	110	20	210	130
Sr(ppm)	650	730	430	630	610	340	260	160	400	250
Rb(ppm)	20	20	30	20	20	100	10	10	10	<10
U(ppm)	1.2								0.7	0.2
Th(ppm)	3.3								3.1	1.7
CIPW normative minerals										
Quartz				8.33			2.45			
Corundum										
Zircon	0.05	0.05	0.03	0.04	0.04	0.04	0.02	<0.01	0.04	0.03
Orthoclase	8.34	9.09	4.76	6.94	6.75	8.63	2.78	1.01	5.35	2.95
Albite	29.44	29.61	24.07	21.77	21.07	27.84	22.60	19.17	29.26	25.25
Anorthite	24.15	23.89	24.87	25.91	24.84	27.49	27.29	34.77	32.36	23.95
Nepheline	3.93	3.30	3.15	4.31	5.92					
Acmite										
Na-metasilicate										
Wollastonite	8.56	8.39	10.66	7.59	9.60	5.36	10.46	11.14	6.07	10.45
Enstatite	6.18	6.17	7.04	5.42	6.80	7.76	12.42	7.57	5.56	13.27
Ferrosilite	1.60	1.42	2.85	1.49	1.96	4.47	9.82	3.15	10.12	9.27
Forsterite	4.77	4.92	9.07	12.33	9.70		3.17	13.42		1.79
Fayalite	1.36	1.24	4.05	3.73	3.09		2.76	6.15		1.38
Magnetite	5.69	5.81	4.98	4.71	4.65	5.38	3.87	2.37	4.14	5.83
Chromite	0.03	0.02	0.06	0.04	0.05	0.02	0.03	0.11	0.01	0.02
Hematite										
Ilmenite	4.52	4.71	3.59	4.58	4.40	4.12	4.18	1.01	3.44	5.03
Apatite	1.42	1.40	0.86	1.16	1.17	0.58	0.62	0.01	1.24	0.80
Mineral partitions										
Di(Wo)	8.56	8.39	10.66	7.59	9.60	5.36	10.46	11.14	6.07	10.45
Di(En)	6.18	6.17	7.04	5.42	6.80	3.22	5.64	7.31	2.20	5.90
Di(Fs)	1.60	1.42	2.85	1.48	1.96	1.85	4.46	3.04	4.01	4.12
Hy(En)						4.54	6.78	0.26	3.36	7.38
Hy(Fs)						2.61	5.36	0.11	6.12	5.15

TABLE 2.--Major element chemical analyses (continued)

Sample No.	175785	165574	165503	165509	165546	165559	165560	165562	165571	165572
Unit symbol	Tgg	Tdr	Tg	Td	Td	Td	Td	Td	Td	Td
Rock type	Diorite (Andesite)	Qz.diorite (Dacite)	Gabbro (Alk.basalt)	Diabase (Alk.basalt)	Rhyolite	Hawaiite	Rhyolite	Diabase (Basalt)	Basalt	Dacite
N. Latitude	20°54.4'	20°47.7'	20°58.4'	20°55.5'	20°44.3'	20°49.0'	20°49.0'	20°49.2'	20°47.7'	20°47.7'
E. Longitude	39°53.2'	39°51.3'	39°35.4'	39°41.5'	39°53.4'	39°51.9'	39°51.9'	39°57.6'	39°51.3'	39°51.3'
SiO_2	57.3	58.4	46.3	46.6	74.3	47.2	72.4	50.9	46.2	59.7
Al_2O_3	14.4	17.8	22.9	20.5	12.2	16.5	13.1	15.6	15.0	16.0
Fe_2O_3	4.0	3.1	3.5	3.7	2.1	11.6	2.0	3.9	3.4	3.7
FeO	5.1	3.4	2.8	4.4	0.1	5.0	0.1	6.3	9.6	3.7
MgO	2.21	1.07	3.95	3.61	0.21	4.75	0.35	4.76	5.39	1.43
CaO	5.59	4.10	13.0	11.9	0.22	9.70	0.55	7.52	7.74	3.19
Na_2O	3.91	6.40	2.88	3.15	4.10	3.50	3.87	3.64	3.54	5.79
K_2O	2.18	1.94	0.34	0.63	3.98	1.33	4.91	1.41	1.15	2.88
LOI	2.08	0.85	3.08	2.23	1.00	1.77	1.31	2.23	2.70	1.16
TiO_2	1.73	0.81	1.02	1.40	0.07	2.01	0.20	1.77	2.40	1.08
P_2O_5	0.58	0.22	0.13	0.23	<0.01	0.24	0.04	0.28	0.46	0.31
MnO	0.19	0.18	0.09	0.13	0.03	0.16	0.03	0.16	0.21	0.14
Total	99.4	98.3	100.1	98.5	98.4	98.3	99.0	98.5	97.8	99.1
Cr(ppm)	30	50	90	80	140	90	80	70	50	50
Zr(ppm)	490	750	50	110	840	190	200	200	190	480
Sr(ppm)	380	400	530	420	<10	300	60	360	420	230
Rb(ppm)	30	20	10	20	290	50	90	30	30	70
U(ppm)	2.1	1.6			13.8				0.3	
Th(ppm)	7.8	3.6			40.6				1.4	
Normative minerals										
Quartz	12.19	2.88			35.29		30.22	1.54		5.70
Corundum					0.77		0.53			
Zircon	0.10	0.16	0.01	0.023	0.17	0.04	0.04	0.04	0.04	0.098
Orthoclase	13.25	11.76	2.08	3.87	24.14	8.17	29.73	8.66	7.17	17.38
Albite	34.02	55.53	22.28	25.65	35.61	27.78	33.55	32.01	31.51	50.04
Anorthite	15.73	14.47	50.14	41.51	1.12	26.38	2.53	22.93	22.73	9.36
Nepheline			1.56	1.12		1.62				
Acmite										
Na-metasilicate										
Wollastonite	3.71	2.05	6.51	7.64		9.19		5.82	6.04	1.98
Enstatite	5.66	2.73	4.52	4.65	0.54	5.37	0.89	12.32	4.87	3.64
Ferrosilite	5.76	4.88	1.45	2.60		3.38		7.57	4.08	5.15
Forsterite			3.95	3.29		4.85			6.48	
Fayalite			1.40	1.99		3.37			5.98	
Magnetite	4.82	3.43	3.77	4.37	1.85	5.29	0.87	4.93	5.17	3.82
Chromite	0.01	0.01	0.02	0.02	0.03	0.02	0.02	0.02	0.01	0.01
Hematite					0.34		1.14			
Ilmenite	3.38	1.58	2.00	2.76	0.14	3.96	0.39	3.49	4.79	2.10
Apatite	1.41	0.53	0.32	0.57		0.59	0.97	0.69	1.15	0.75
Mineral partitions										
Di(Wo)	3.71	2.05	6.51	7.64		9.19		5.82	6.05	1.99
Di(En)	1.81	0.75	4.52	4.65		5.37		3.43	3.19	0.82
Di(Fs)	1.84	1.34	1.45	2.56		3.38		2.11	2.67	1.17
Hy(En)	3.85	1.98			0.54		0.89	8.89	1.68	2.82
Hy(Fs)	3.92	3.54						5.46	1.41	3.99

TABLE 2.--Major element chemical analyses (continued)

Sample No.	165597	165627	165661	165691	165717	165756	165811	165857	165881	165882
Unit symbol	Td	Td	Td	Td	Td	Td	Td	Td	Td	Td
Rock type	Rhyolite	Comendite	Diabase (Hawaiite)	Basalt	Rhyolite	Dacite	Rhyolite	Rhyolite	Basalt	Hawaiite
N. Latitude	20°46.4'	20°48.6'	20°56.8'	20°47.5'	20°38.1'	20°54.5'	20°43.3'	20°45.4'	20°52.4'	20°54.2'
E. Longitude	39°53.9'	39°54.0'	39°40.5'	39°39.5'	39°53.1'	39°33.9'	39°53.7'	39°51.6'	39°56.5'	39°53.8'
SiO_2	65.7	71.2	46.6	46.6	70.1	72.6	74.0	66.4	49.0	47.0
Al_2O_3	15.1	11.3	15.9	16.1	13.4	13.1	12.2	13.9	14.0	17.3
Fe_2O_3	2.1	4.3	3.1	3.3	3.3	1.5	1.7	4.2	4.7	3.8
FeO	2.0	0.7	5.3	7.3	0.2	0.9	0.1	0.7	7.6	7.3
MgO	0.61	0.22	7.44	8.27	0.28	0.67	0.17	0.26	5.14	4.01
CaO	1.61	0.31	9.21	10.0	1.07	2.08	0.40	1.02	8.29	8.34
Na_2O	5.14	5.11	3.35	2.60	3.33	3.59	4.13	5.77	2.85	3.99
K_2O	3.79	4.13	1.21	0.30	4.52	2.91	4.16	3.87	1.59	1.15
LOI	1.89	0.85	3.77	2.16	2.39	1.16	1.47	1.77	1.93	2.62
TiO_2	0.48	0.26	1.51	1.20	0.25	0.29	0.08	0.38	2.62	2.49
P_2O_5	0.11	0.01	0.41	0.14	0.02	0.05	<0.01	0.03	0.34	0.42
MnO	0.08	0.09	0.14	0.17	0.05	0.05	0.02	0.13	0.19	0.17
Total	98.6	98.5	97.9	98.3	98.9	98.9	98.4	98.4	98.2	98.7
Cr(ppm)	50	120	301	130	70	140	160	70	70	30
Zr(ppm)	540	1530	160	30	680	100	350	820	240	170
Sr(ppm)	170	<10	510	220	10	390	<10	10	260	560
Rb(ppm)	50	130	30	20	110	40	170	80	50	40
U(ppm)		5.2	0.9						0.8	0.59
Th(ppm)		17.0	2.7						3.3	1.20
Normative minerals										
Quartz	17.12	25.76			31.36	35.33	33.93	15.46	2.48	
Corundum					1.17	0.39	0.18			
Zircon	0.02	0.31	0.03	0.01	0.14	0.02	0.07	0.17	0.05	0.04
Orthoclase	23.14	24.99	7.59	1.85	27.70	17.59	25.33	23.68	9.76	7.08
Albite	44.95	35.97	28.09	22.91	29.22	31.07	36.01	50.55	25.05	35.17
Anorthite	7.17		26.28	32.67	5.37	10.22	2.05	0.62	21.51	26.98
Nepheline			1.08							
Acmite		5.21								
Na-metasilicate		0.56								
Wollastonite	0.14	0.63	8.09	7.53				1.84	7.89	5.54
Enstatite	1.57	0.56	5.76	11.12	0.72	1.71	0.44	0.67	13.30	8.55
Ferrosilite	1.69	5.45	1.61	5.74	1.13	1.62		3.35	7.76	
Forsterite			9.74	7.24						1.30
Fayalite			3.00	4.12						
Magnetite	2.97		4.63	4.08	2.63	1.34	0.56	2.82	6.21	5.78
Chromite	0.01	0.03	0.07	0.03	0.02	0.03	0.04	0.02	0.02	0.01
Hematite							1.25			3.62
Ilmenite	0.94	0.51	3.04	2.37	0.49	0.56	0.16	0.75	5.16	4.93
Apatite	0.27	0.02	1.03	0.35	0.05	0.12		0.07	0.84	1.04
Mineral partitions										
Di(Wo)	0.14	0.63	8.08	7.53				1.84	7.89	5.54
Di(En)	0.07	0.07	5.76	4.67				0.33	4.72	4.79
Di(Fs)	0.07	0.63	1.61	2.41				1.66	2.76	
Hy(En)	1.50	0.50		6.44	0.72	1.71	0.44	0.34	8.57	3.76
Hy(Fs)	1.63	4.82		3.33	1.13	1.63		1.69	5.00	

TABLE 2.--Major element chemical analyses (continued)

Sample No.	175780	175834	165575	165791	175825	165502	165662	165680	165683	165714
Unit symbol	Td	Td	Td	Td	Td	Tv	Tv	Tv	Tv	Tv
Rock type	Diabase (Basalt)	Basalt	Basalt	Diabase (Basalt)	Trachyte	Rhyolite	Rhyolite	Rhyolite	Dacite	Perlite (Rhyolite)
N. Latitude	20°48.8'	20°39.3'	20°47.7'	20°57.1'	20°54.6'	20°44.6'	20°56.7'	20°55.2'	20°53.0'	20°44.5'
E. Longitude	39°52.9'	39°47.5'	39°51.3'	39°41.4'	39°42.0'	39°37.9'	39°40.4'	39°39.1'	39°34.3'	39°38.0'
SiO_2	47.0	46.2	46.6	47.1	57.8	70.0	65.8	64.0	71.8	72.3
Al_2O_3	14.8	15.1	15.9	17.8	17.5	14.2	14.3	16.8	13.4	11.7
Fe_2O_3	5.6	4.4	3.7	4.4	3.4	2.4	5.0	4.6	1.5	1.2
FeO	7.7	5.6	8.6	6.5	2.6	0.3	0.7	0.2	1.1	0.8
MgO	5.28	10.7	5.77	4.16	0.69	0.41	0.39	0.53	0.83	0.11
CaO	9.00	9.41	7.91	10.4	2.11	0.61	1.91	0.36	3.34	0.37
Na_2O	3.39	1.89	3.22	2.76	6.94	3.81	4.86	5.86	3.96	2.70
K_2O	0.81	0.20	1.12	0.96	4.46	4.89	3.99	4.24	1.23	4.22
LOI	2.08	4.70	3.16	1.62	1.93	2.62	0.62	1.77	1.23	5.77
TiO_2	2.53	0.84	2.20	2.10	0.50	0.18	0.43	0.38	0.27	0.14
P_2O_5	0.52	0.12	0.43	0.30	0.10	0.02	0.07	0.06	0.05	<0.01
MnO	0.21	0.17	0.18	0.16	0.15	0.05	0.05	0.11	0.05	0.04
Total	99.0	99.4	98.8	98.3	98.2	99.6	98.1	99.0	98.8	99.3
Cr(ppm)	80	310	60	40	30	30	80	40	150	30
Zr(ppm)	190	40	30	10	100	450	910	590	120	490
Sr(ppm)	400	170	530	410	200	70	100	110	500	<10
Rb(ppm)	20	<10	190	160	560	100	50	100	30	120
U(ppm)	0.4	<0.1								3.6
Th(ppm)	1.7	<0.5								7.9
Normative minerals										
Quartz	3.91					28.01	17.11	11.28	36.24	41.41
Corundum						1.63		2.12		2.15
Zircon	0.03	0.01	0.04	0.03	0.12	0.09	0.19	0.12	0.03	0.11
Orthoclase	2.93	1.25	6.92	5.87	27.42	29.82	24.23	25.84	7.45	26.62
Albite	25.21	16.93	28.48	24.36	50.14	33.27	42.27	51.14	34.34	24.39
Anorthite	23.99	34.01	26.78	34.43	3.56	2.99	5.57	1.44	15.53	1.96
Nepheline					5.93					
Acmite										
Na-metasilicate										
Wollastonite	10.41	6.09	4.72	7.08	2.78		1.54		0.47	
Enstatite	15.82	19.53	8.67	10.55	0.77	1.05	1.00	1.36	2.12	0.29
Ferrosilite		7.78	5.69	7.20	2.14	0.21	4.19	2.99	1.51	1.55
Forsterite		6.08	4.45	0.12	0.71					
Fayalite		2.67	3.22	0.09	2.18					
Magnetite	6.04	3.59	5.61	5.40	3.02	2.51	2.88	2.81	1.64	1.24
Chromite	0.02	0.07	0.01	0.01	0.01	0.01	0.02	0.01	0.03	0.01
Hematite	5.84									
Ilmenite	5.03	1.69	4.37	4.13	0.99	0.35	0.84	0.74	0.53	0.28
Apatite	0.81	0.30	1.07	0.74	0.25	0.05	0.17	0.15	0.12	
Mineral partitions										
Di(Wo)	10.41	6.09	4.72	7.08	2.78		1.54		0.47	
Di(En)	9.00	4.04	2.72	4.03	0.77		0.32		0.26	
Di(Fs)		1.61	1.78	2.14	2.14		1.34		0.19	
Hy(En)	6.82	15.50	5.95			1.05	0.68	1.36	1.86	0.29
Hy(Fs)		6.17	3.91			0.21	2.86	2.99	1.32	1.55

TABLE 2.--Major element chemical analyses (continued)

Sample No.	165766	165767	175771	165768	165772	175826
Unit symbol	Tv	Tv	Tv	Tv	Tv	Tv
Rock type	Trachyte	Alk.basalt	Basalt	Basalt	Basalt	Trachy-basalt
N. Latitude	20°57.9'	20°57.5'	20°16.8'	20°58.1'	20°58.4'	20°54.6'
E. Longitude	39°36.7'	39°37.2'	40°20.4'	39°37.0'	39°38.3'	39°42.0'
SiO_2	53.8	45.1	46.6	44.0	46.8	43.7
Al_2O_3	19.3	13.8	16.2	16.9	17.0	19.1
Fe_2O_3	3.2	5.8	4.1	8.4	3.3	4.9
FeO	1.8	6.8	6.8	2.8	7.1	4.6
MgO	0.56	5.28	8.71	6.02	5.89	4.91
CaO	2.78	10.7	10.1	8.80	8.73	9.04
Na_2O	7.25	3.43	2.64	2.48	3.06	2.66
K_2O	4.80	0.18	0.28	1.43	1.01	1.63
LOI	4.39	4.77	1.70	5.08	2.85	5.62
TiO_2	0.62	2.16	1.21	2.71	2.15	2.23
P_2O_5	0.12	0.36	0.14	0.35	0.39	0.37
MnO	0.18	0.20	0.18	0.18	0.16	0.15
Total	98.7	98.5	98.8	99.3	98.5	99.0
Cr(ppm)	10	50	130	130	40	40
Zr(ppm)	490	150	60	20	30	30
Sr(ppm)	580	420	260	580	520	540
Rb(ppm)	100	10	10	210	190	140
U(ppm)		0.4				
Th(ppm)		1.2				
Normative minerals						
Quartz						
Corundum						
Zircon	0.10	0.03	0.01	0.04	0.04	0.03
Orthoclase	30.07	1.14	1.71	9.02	6.24	10.34
Albite	35.82	29.90	23.08	22.39	27.08	23.91
Anorthite	6.30	23.22	32.57	32.82	31.03	37.98
Nepheline	15.83	0.60				0.14
Acmite						
Na-metasilicate						
Wollastonite	3.13	12.94	7.62	4.73	4.84	3.16
Enstatite	1.13	7.16	9.49	8.72	10.02	2.21
Ferrosilite	2.07	5.29	4.72	2.61	4.82	0.69
Forsterite	0.25	4.83	9.06	5.10	3.73	7.65
Fayalite	0.60	3.93	4.96	1.69	1.98	2.63
Magnetite	3.26	5.67	4.06	6.50	5.00	5.76
Chromite	<0.01	0.01	0.03	0.03	0.01	0.01
Hematite						
Ilmenite	1.25	4.38	2.37	5.49	4.27	4.55
Apatite	0.30	0.91	0.34	0.89	0.97	0.94
Mineral partitions						
Di(Wo)	3.13	12.94	7.62	4.73	4.84	3.17
Di(En)	1.13	7.16	4.78	3.33	3.07	2.21
Di(Fs)	2.07	5.29	2.38	1.00	1.47	0.69
Hy(En)			4.71	5.39	6.96	
Hy(Fs)			2.34	1.62	3.35	

GUMAYQAH COMPLEX

Thick (10- to 100-m) and widely-spaced gabbro to monzogabbro dikes intrude the Proterozoic rocks of the quadrangle in a diffuse, northwest-trending regional swarm (figs. 1 and 2). The dikes are typically coarse grained in the centers and have fine grained (diabasic) margins. Wall rocks immediately adjacent to the dikes are commonly recrystallized to hornfels. These factors produce resistant dike margins and easily weathered cores, such that a dual-rib or "railroad track" weathering pattern is produced (fig. 5).

Individual dikes of the Gumayqah complex have been mapped for as much as 50 kilometers and form prominent aeromagnetic lineaments that allow extension of dike traces under alluvium. Similar, northwest-trending, thick gabbro dikes occur throughout the coastal provinces of Saudi Arabia and into the Sinai Peninsula, where they show offset across the Gulf of Aqaba (Blank, 1977; Bartov and others, 1980). Dikes of the Gumayqah complex were termed "Continental dikes" by Coleman and others (1979).

Gumayqah dikes crosscut the Damm dike complex southeast of Harrat Tuffil, and they are overlain by Miocene alkali basalt at Harrat ad Damm. Whole-rock K-Ar dates on some of the Gumayqah dikes are anomalously old (100-200 Ma, table 1) because of contamination by excess radiogenic argon from Precambrian host rocks. However, one of the gabbro dikes north of Jabal Basham is dated by plagioclase K-Ar at 21.7±0.5 Ma and by clinopyroxene K-Ar at 24.4±1.2 Ma. Correlative thick northwesterly-trending dikes along the margins of the Red Sea are dated at about 18-22 Ma in other areas (Bartov and others, 1980 Schmidt and others, 1982).

MIOCENE ALKALI BASALT

Miocene alkali basalt forms Harrat ad Damm and small flow remnants north of Jabal Sita. The rock consists of fine-grained, intergranular to subophitic or locally diktytaxitic olivine, olivine-plagioclase, and clinopyroxene-olivine-plagioclase porphyritic to microporphyritic basalt. The basalt at Harrat ad Damm is dated by clinopyroxene K-Ar at 11.3±0.6 Ma (table 1). The overall Harrat morphology (fig. 2) suggests that the lava flow once filled a broad paleovalley that had a trellis drainage pattern on a gently southwest sloping Precambrian basement surface. The volcanic field is now topographically inverted owing to the more rapid erosion of adjacent basement rocks.

BATHAN FORMATION

The Bathan formation was defined by Hadley and Fleck (1980) for a moderately tilted section of indurated conglomerate and sandstone exposed near Wadi al Lith in the southeastern part of the quadrangle. The Bathan is a terrigenous clastic deposit that consists of boulder and pebble conglomerate and subordinate beds of coarse-grained sandstone. The conglomerate contains angular to subrounded clasts, typically a few centimeters to a half meter in diameter. Clasts of Precambrian metarhyolite, metabasalt, metadiabase, and various granitic rocks predominate, but subordinate olivine-basalt, metadiabase, plagiogranite(?), and hornblende-gabbro clasts probably date from the Tertiary.

Figure 5.--*Aerial view of Gumayqah complex gabbro dike in the east-central part of the Al Lith quadrangle. Dike is approximately 60 meters wide. Low-angle view is to the southeast and shows coarse-grained core of dike exposed between resistant chilled margins and hornfels host rock.*

A small exposure of boulder and cobble lag at Harrat Tuffil is correlated with the Bathan formation. This deposit overlies rhyolite of the Sita formation (dated at 20.3±3.6 Ma and correlated with the rhyolite at Jabal abu Shidad that is dated at 19.2±0.9 Ma, figure 2 and table 1) and underlies Pliocene alkali basalt (3.25±0.05 Ma). The Bathan has not been recognized below the Miocene alkali basalt (11.3±0.6 Ma) at Harrat ad Damm.

The Bathan was assigned a Pliocene age by Hadley and Fleck (1980), who related the deposition and subsequent tilting of the Bathan to Pliocene tectonics of the Red Sea basin and uplift of the Red Sea escarpment. The Bathan formation is also thought by Schmidt and others (1982) to record the first major and rapid uplift of the Red Sea escarpment. The stratigraphic relations and radiometric dating described above bracket the Bathan between 3.2 and about 20 Ma (or possibly between 3.2 and about 11 Ma).

PLIOCENE ALKALI BASALT

Alkali basalt is exposed as a shield volcano at Harrat Tuffil. The unit is composed of fine-grained, intergranular basalt and olivine, olivine-plagioclase, and clinopyroxene-olivine-plagioclase porphyritic to glomeroporphyritic basalt. Poorly preserved flow fronts, channels, and differences in phenocryst assemblages and abundances indicate that several distinct flows are present at Harrat Tuffil. A single flow is mapped for about 12 kilometers south from the eruptive center and probably fills a paleostream channel.

The lava is chemically similar to the Miocene alkali basalt of Harrat ad Damm and to some alkali basalts in the Damm dike complex. Both the Miocene and Pliocene basalts of the Lith region are similar in chemistry and petrography to the voluminous alkali olivine basalts that make up most of the Tertiary and Quaternary flood basalt fields of inland and coastal Arabia (Coleman and others, 1983).

The upper flow in the vent area of Harrat Tuffil is dated by whole-rock K-Ar at 3.25±0.05 Ma (table 1). The basalt unconformably overlies conglomerate of the Bathan formation, rhyolite of the Sita formation, and Proterozoic gneiss and granite.

PETROLOGY AND GEOCHEMISTRY

Chemical analyses of Tertiary rocks from the Al Lith region are presented in tables 2 and 3 and rock names are assigned on a volatile-free basis using the method of Irvine and Baragar (1971). Strontium isotopic initial ratios are calculated for seven representative samples and are listed in table 4. The analyses reported here are part of a reconnaissance geochemical study done in support of regional geologic mapping (Pallister, 1992a-b, unpub. data; 1986). The intent herein is to overview the major geochemical features of the Tertiary rocks and to explain how these data and the geologic history of the region constrain petrologic models for Red Sea rift magmatism.

As noted in the unit descriptions, both the Sita volcanic rocks and the Damm dikes have transitional subalkaline to alkaline chemistry (fig. 6). There is no obvious time progression from mafic to felsic or from alkaline to subalkaline

TABLE 3.--Rare-earth element INAA data for rocks from the Al Lith region

[Abundances in ppm. Volcanic rock names defined as in Table 1. Locality coordinates given in Table 1, except for sample 165614 (20°50.0' N. X 39°50.4' E.). Sample numbers followed with asterisks were analyzed by J. Budahn and R. J. Knight of the U.S. Geological Survey. Other samples analyzed by X-ray Assay Laboratories, Don Mills, Ontario, Canada.]

Sample No.	165006*	165571	165881*	175780	165546*	165882*	165661*	165627	175834	175764
Unit Symbol	Tb,	Td	Td	Td	Td	Td	Td	Td	Td	Tgg
Rock Type	Hawaiite	Basalt	Basalt	Diabase (Basalt)	Rhyolite	Hawaiite	Diabase (Hawaiite)	Comendite	Basalt	Diabase (Basalt)
La	30.5	18.0	29.0	21.0	61.0	14.7	21.1	70	4.6	30.0
Ce	61	45	64	47	95	34	42	183	11	67
Nd	32	28	36	29	35	22	23	70	8	40
Sm	6.7	7.5	9.1	8.0	10.2	5.9	5.0	17.0	2.7	10.0
Eu	2.2	2.7	3.0	2.4	0.08	2.0	1.65	1.9	1.1	3.3
Gd	6.7				8.3	5.8	4.6			
Tb	0.98	1.2	1.5	1.2	2.37	1.0	0.73	3.2	0.7	1.5
Dy	5.8	7.2	7.8	7.7	22.7	6.5	4.5	19.7	3.8	9.5
Tm					4.10	0.47	0.37			
Yb	2.6	3.8	3.8	3.7	35.9	2.8	2.4	17.0	2.5	4.5
Lu	0.40	0.53	0.58	0.53	5.56	0.44	0.37	2.50	0.40	0.66

Sample No.	175785	175776	165574*	165614	165767	165714*
Unit Symbol	Tgg	Tgg	Tdr	Tan	Tv	Tv
Rock Type	Diorite (Andesite)	Diabase (Basalt)	Qz.diorite (Andesite)	Gabbro	Alk.basalt	Perlite (Rhyolite)
La	57.0	18.0	29.1	37.0	16.0	48.0
Ce	120	39	66	82	39	106
Nd	70	25	37	45	25	59
Sm	16.0	6.5	8.6	11.0	6.8	13.9
Eu	4.4	2.5	4.3	3.6	2.4	1.14
Gd			8.3			14.5
Tb	2.2	1.1	1.37	1.6	1.3	2.6
Dy	14.0	5.9	8.3	9.3	7.4	16.4
Tm			0.82			1.55
Yb	6.8	3.0	5.0	6.3	3.9	9.7
Lu	0.94	0.47	0.82	0.99	0.58	1.43

TABLE 4.--Strontium isotopic data for rocks from the Al Lith region

[Detection limits for Rb and Sr are 10 ppm (Table 2). Theoretical limits for initial $^{87/86}Sr$ are based on Sr abundances of 1 and 10 ppm. $^{87}Rb/^{86}Sr$ and initial $^{87/86}Sr$ ranges calculated based on Rb concentrations of 1 and 10 ppm. Isotopic analyses by Australian Mineral Development Laboratories (AMDEL), Frewville, South Australia. Ages based on K-Ar geochronology and geologic correlations. Where age ranges only are known, initial $^{87/86}Sr$ ratios are calculated for the two extremes.]

Unit Symbol	Sample Number	Rock type and description	$^{87/86}Sr$(Initial)	Age(Ma)	$^{87/86}Sr$(Measured)	Sr(ppm)	Rb(ppm)	Rb/Sr	$^{87}Rb/^{86}Sr$
Tb_2	165006	Aphyric hawaiite, flow at Harrat Tuffil	0.7031	3.25	0.70310 ± 0.00007	650	20	0.031	0.089
Tgg	175785	Diorite, andesite composition, intrudes P€ metabasalt and gneiss	0.7047	20	0.70474 ± 0.00005	380	30	0.079	0.228
Tgg	175764	Gabbro, tholeiite composition, intrudes P€ metabasalt	0.7045	18-22	0.70452 ± 0.00006	400	10	0.025	0.072
Td	165881	Basalt (tholeiite) dike, intrudes granite gneiss	0.7042-0.7047	80-20	0.70483 ± 0.00004	260	50	0.19	0.556
Td	165882	Hawaiite dike, plagioclase megacrystic, intrudes granite gneiss and schist	0.7034-0.7036	80-20	0.70362 ± 0.00008	560	40	0.071	0.207
Td	175834	Basalt sill, Mg-rich tholeiite, intrudes dolomite	0.7035-0.7037	80-20	0.70373 ± 0.00007	170	<10	<0.06	0.017-0.170
Tv	165714	Perlite lava flow, rhyolite composition	0.6943-0.7042	20	0.71409 ± 0.00014	<10	120	>12	34.7-347

magmatism; mutually intrusive relations among the various magma types are observed in the Damm dike complex. The dikes and volcanic rocks consist of a bimodal mafic-felsic suite with a Daly gap between about 53% and 68% SiO_2. Tholeiitic basalt and dacite to rhyolite predominate among the subalkaline rocks; alkali basalt to hawaiite and trachyte predominate among the alkaline rocks (fig. 7). Most of the alkaline rocks have $Na_2O/K2O$ ratios greater than 1.0 and are members of the sodic-alkali basalt series of Irvine and Baragar (1971). The basalts range from nepheline- to quartz-normative and the rhyolites typically are peraluminous, with molar Al_2O_3/Na_2O+K_2O+CaO ranging from slightly more than 1.0 to 1.2 and variable amounts of normative corundum (0.2 to 2.2% - table 2). The peraluminous character of the rhyolites may, at least in part, be a consequence of alteration of volcanic glass as described by Chayes (1970).

The Al Lith rocks have overlapping rare-earth element (REE) patterns with negative slopes and most show considerable light rare-earth element (LREE) enrichment (fig. 8). The similar, strongly negative slopes of the patterns for the basaltic rocks and relatively low initial $^{87}Sr/^{86}Sr$ (see below) suggest that these rocks were derived from similar mantle sources that were not depleted in LREE (Gast, 1968). A high-MgO (10.7%, table 2) tholeiitic basalt sill that intrudes Jurassic(?) dolomite southeast of Harrat Tuffil is clearly anomalous, because it has a flat REE pattern at about 13 times chondrite abundance.

The best preserved record of rift magmatism in the region is found in the Damm dike complex. Because dike intrusion took place over a relatively long period, it is likely that the swarm collectively represents a number of separate magmatic events. Unfortunately, the parallelism of the swarms does not allow discrimination of coeval packages of dikes (representing individual episodes of intrusion) within the long-lived complex. As a consequence, it has not been possible to select coeval subsets of the suite for more detailed geochemical and petrologic studies. Quantitative modeling of the effect of crystal fractionation and assimilation on the trace- and major-element compositions of the rift-related igneous rocks is also complicated by the fragmentary volcanic stratigraphy and by the degree of alteration of the rocks. Many of the rocks have undergone greenschist metamorphism which produced secondary hydrous mineral assemblages (note high LOI values in table 2). There is considerable scatter superimposed on "magmatic-type" trends in major-element variation diagrams for the Al Lith rocks. But, the general features of the major-element data (bimodality and presence of alkaline and subalkaline compositions) are primary, as evidenced by the presence of fresh samples in each group. In spite of these difficulties, several qualitative observations are apparent from the reconnaissance geochemical data.

DISCUSSION

BIMODALITY

Bimodality is most commonly attributed to either anatexis of crustal rocks by mantle-derived basaltic melts or to low-pressure fractionation away from a thermal divide (Steinthorsson and others, 1985). The observed mafic-felsic bimodality of Red Sea rift rocks has traditionally been attributed to melting of crustal material (Schmidt and others, 1982; Coleman, 1984b). The effect of Precambrian crustal contamination is seen in anomalously old K-Ar dates (indicating excess radiogenic Ar) from Gumayqah complex dikes (table 1). Melting

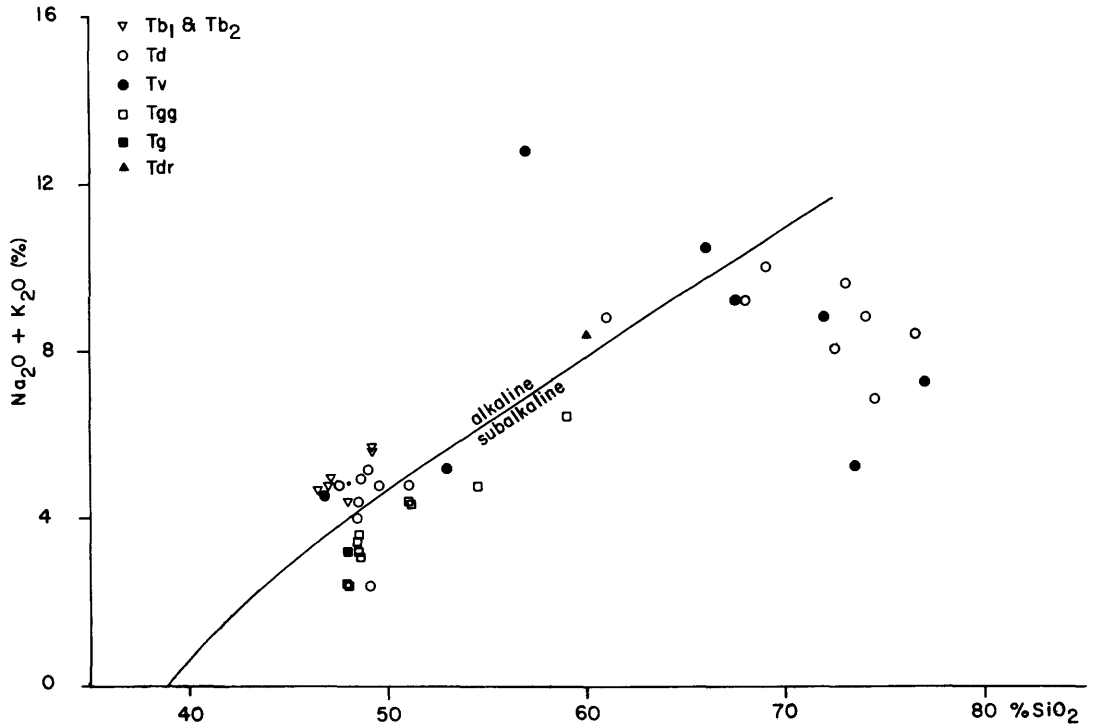

Figure 6.--*Silica-combined alkali variation diagram for rocks from the Al Lith region showing the alkaline-subalkaline division of Irvine and Baragar (1971).*

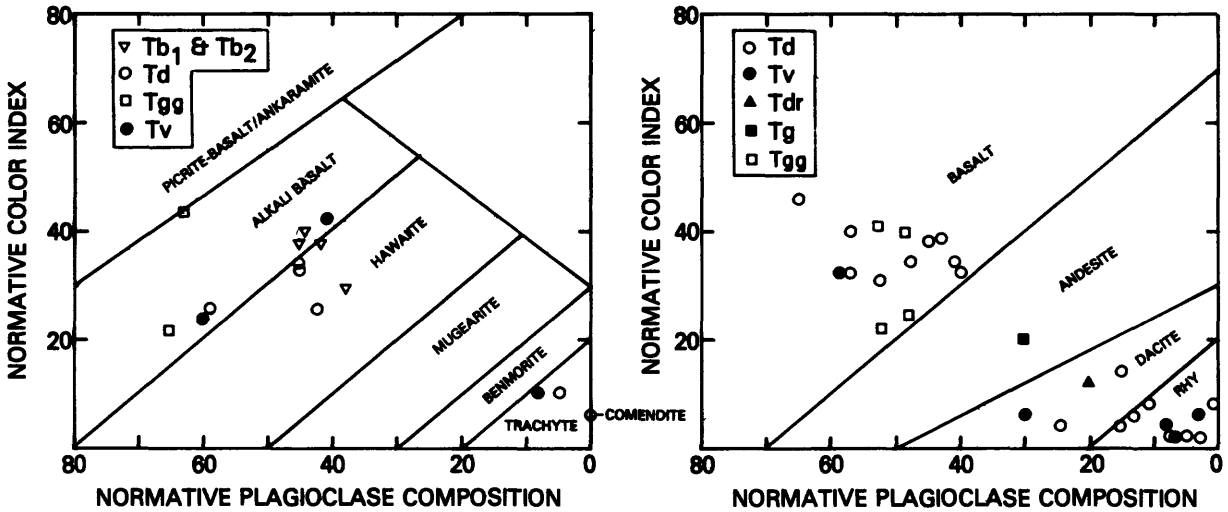

Figure 7.--*Volcanic rock classification diagrams for rocks from the Al Lith region based on the method of Irvine and Baragar (1971). Rocks classified as alkaline are shown on left; subalkaline on right.*

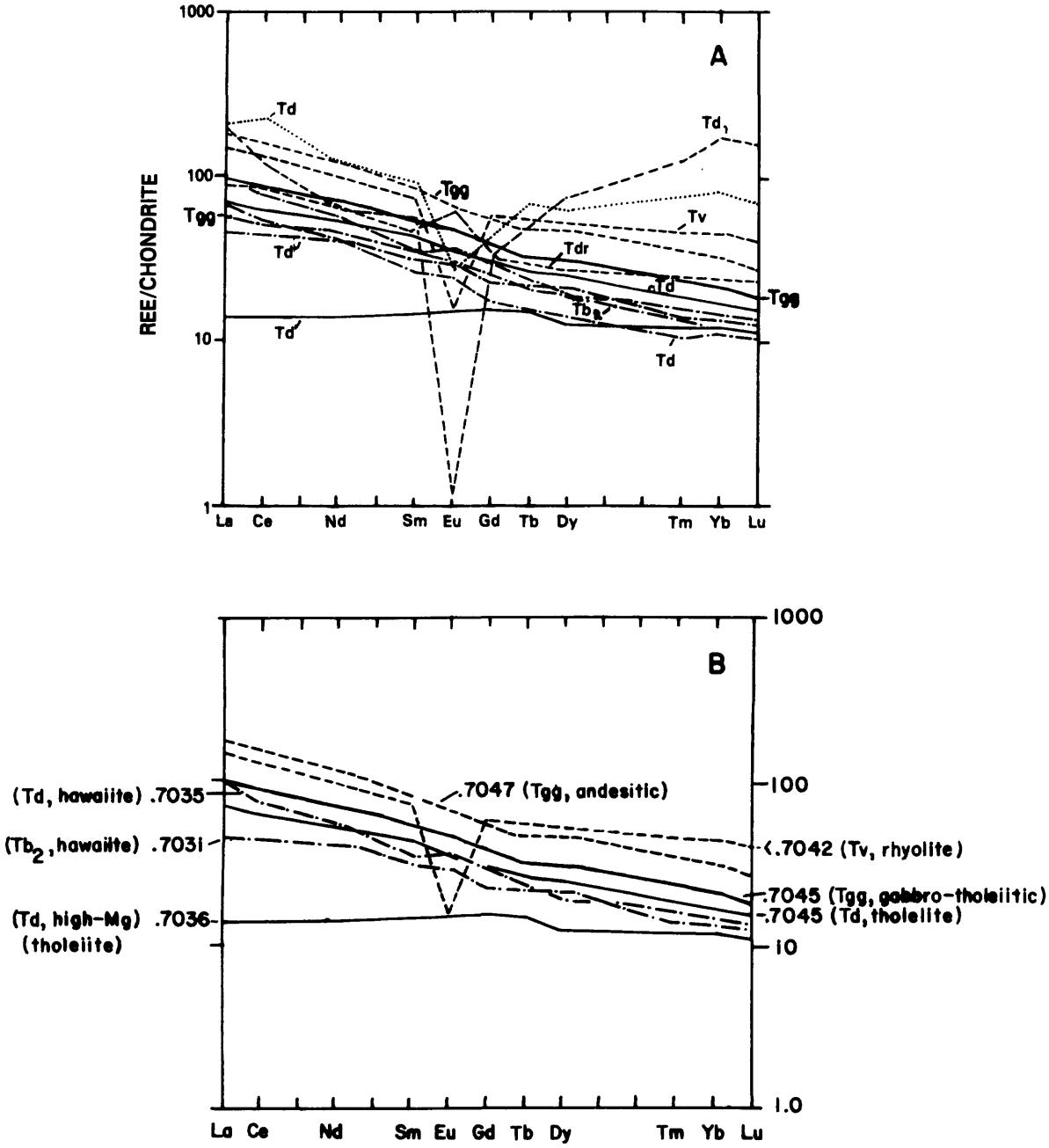

Figure 8.--*Chondrite-normalized rare-earth element diagrams for rocks from the Al Lith region. Unit symbols are defined in Figure 2. Initial $^{87}Sr/^{86}Sr$ ratios (values from table 5) are also given in (B) for samples for which both Sr isotopic, and REE data are available. Line types in both (A) and (B) are as follows: solid = subalkaline and mafic, dashed = subalkaline and intermediate to felsic, dot-dashed = alkaline and mafic, dotted = alkaline and felsic.*

of continental crust is also suggested by the abundance of felsic differentiates in other parts of the Red Sea-Afar region (such as Yemen, where the basalt:rhyolite ratio reaches 1:1 (Grolier and Overstreet, 1978; Coleman, 1984a).

Proterozoic granite gneiss is host to the eastern part of the Gumayqah dike swarm (fig. 2) and is a major batholithic component of the upper crust in the Al Lith region. It therefore represents a potential contaminant to the Tertiary magmas. The granite gneiss has Tertiary (30 Ma) $^{87}Sr/^{86}Sr$ ratios of 0.708 to 0.713 and Sr abundances that range from 244 to 507 ppm (from data in Fleck and Hadley, 1982). Sufficient contamination by the gneiss to produce either dacite-rhyolite or trachyte-comendite from mantle-derived basaltic melts, or an origin involving direct melting of the Proterozoic granite gneiss would have produced elevated initial $^{87}Sr/^{86}Sr$ ratios. But little, if any, elevation of initial $^{87}Sr/^{86}Sr$ is apparent in rhyolite from the Al Lith area (table 4).

Sita formation rhyolite from an eroded lava flow near Harrat Tuffil has a REE pattern that is approximately parallel to many of the basaltic rocks and has a moderate negative Eu anomaly. A sample of the lava (165714, table 4) has an initial $^{87}Sr/^{86}Sr$ ratio less than or equal to 0.7042 (based on an age of 20 Ma - table 1). This is similar to the initial $^{87}Sr/^{86}Sr$ for subalkaline basalt from the Damm dike complex (0.7042-0.7047, sample 165881, table 4). Crystal fractionation of basalt by removal of plagioclase and other observed phenocryst phases to produce the rhyolite might be suggested, but would be incompatible with the available major-element chemistry (note that Na_2O in the rhyolite is comparable to that in the analyzed subalkaline basalts (table 2)).

Rhyolite from the Damm dike complex shows extreme Eu depletion and strong HREE enrichment relative to the Sita rhyolite (compare 165714 and 165546 - table 3 and fig. 8). This rock also is not readily explained by simple low-pressure crystal fractionation. No combination of the common phenocryst minerals in the Tertiary rocks (olivine, pyroxenes, hornblende, biotite, oxides, plagioclase, quartz, sanidine) would produce the required HREE-enrichments by crystal fractionation (see reviews of trace element partitioning by Irving (1978), Henderson (1984), and Irving and Frey (1984)). Enrichment of all the REE by major-phase fractionation followed by depletion of the LREE by accessory-phase fractionation (e.g., the removal of apatite and sphene, the latter to account for the middle-REE depletions) could produce relative HREE enrichment, but the high absolute abundance of HREE (table 3) in the rhyolite favors a mechanism by which HREE are added to the system. In any case, parent magma for the rhyolite must have been derived from a source with plagioclase in the residuum to account for the extreme negative Eu anomaly.

Enrichment of HREE is generally regarded as a fingerprint of liquid-state diffusion (Hildreth, 1979) and has been attributed to volatile transfer in flourine-rich peraluminous rhyolitic systems (Christiansen and others, 1984). Although flourine has not been analyzed in the Al Lith rhyolites, rubidium enrichment accompanies HREE elevation in flourine-rich rhyolites (Christiansen and others, 1984), but is not apparent in table 2. Although a diffusion-based process may account for the HREE-enrichment in the rhyolite, an intriguing alternative exists. Complete melting or physical addition of a HREE-enriched phase could also account for the anomalous REE patterns of the rhyolite. A source with residual plagioclase and containing a HREE-enriched phase would be required.

Zircon, garnet, and some amphiboles are the only common crustal minerals that are strongly HREE enriched. Zircon has high partition coefficients for HREE ranging from about 10 to 100 (Nagasawa, 1970; Watson, 1980; Irving and Frey, 1984) or to 600 in high-silica rhyolites (Mahood and Hildreth, 1983), but unrealistically large amounts of zircon addition (in excess of 20%) would be required to produce the large HREE enrichments of about 170 times chondrite (fig. 8) and would be obvious in the Zr content of the rhyolite.

Anatexis of a low $^{87}Sr/^{86}Sr$ plagioclase and garnet ± amphibole-bearing aluminous assemblage of middle to lower crustal rocks could explain the unusual HREE enrichments. Amphibole shows variable degrees of middle and heavy REE enrichment (partition coefficients increase with increasing silica content of the host - Green and Pearson, 1985) and garnet is highly enriched in HREE (Irving, 1978), but (given equilibrium) either phase would have to be melted out of the host to contribute HREE to the melt.

Garnet is generally regarded as a refractory phase, probably because of the role of pyrope in basalt genesis and as a primary constituent of eclogite and some peridotites. However, garnets of many crustal granulites and gneisses are almandine- or spessertine-rich and may be early-melting phases. Almandine melts incongruently to various combinations of hercynite, cordierite, quartz, and liquid at temperatures between 1088° and 1200° and pressures between 0.1 MPa (1 atmosphere) and 2.0 GPa (20 kb) (Keesman and others, 1971) and garnet in quartzofeldspathic granulite xenoliths from Kilbourne hole is the phase most affected by disequilibria melting (Padovani and Carter, 1981). Garnet is also an early-melting component in experimental studies of some granitic and tonalitic rocks (e.g. Stern and Wyllie, 1981; Huang and Wyllie, 1981). Almandine partition coefficients yield REE patterns parallel to those from pyrope but up to an order of magnitude higher and with large negative Eu-anomalies; spessertine is strongly enriched in HREE (about 5000 times chondrite) and shows extreme Eu depletion (Irving and Frey, 1978).

A crustal melting model in which garnet is melted out of the residuum is an alternative explanation for the unusual HREE-enriched rhyolite from the Damm dike complex, as well as for the origin of similar HREE-enrichment in peraluminous granites. Melting of an almandine-rich garnet would contribute HREE to the liquid without appreciably increasing the Eu abundance, a relationship needed to explain genesis of the Damm dike complex rhyolite sample. It is suggested that the HREE-enrichment of peraluminous rhyolites and granites, where not coupled with evidence of volatile transfer (such as the Fl-enrichments seen in topaz rhyolites), and where combined with very large Eu depletion, may indicate complete melting (or reaction) of almandine-or spessartine-rich garnet in source (or contaminant) rocks.

ALKALINITY

Initial $^{87}Sr/^{86}Sr$ ratios of the Tertiary volcanic and hypabyssal rocks range from 0.7031 to 0.7047 and overlap the range observed in the Cenozoic alkali flood basalts of Arabia (Coleman and others, 1977; 1983). The subalkaline and alkaline rocks of the Al Lith area do not show systematic differences in initial $^{87}Sr/^{86}Sr$ or in REE patterns (table 4, fig. 8*B*), indicating that the transition from subalkaline to alkaline compositions was not caused by upper-crustal contamination. In addition, variation of initial $^{87}Sr/^{86}Sr$ with respect to Sr

abundance and Rb/Sr (table 4) is not systematic within the limited data set reported herein, and cannot be explained by simple assimilation or combined assimilation-fractional crystallization models involving a radiogenic and/or isotopically uniform contaminant. The observed range in initial $^{87}Sr/^{86}Sr$ is similar to the range for oceanic islands with oceanic-mantle source regions (see summaries in Faure and Powell, 1972; Staudigel and others, 1984) and is attributed to mantle heterogeneity and possibly lower-crustal assimilation rather than upper-crustal contamination.

The most likely explanations for the variation in alkalinity of the mafic rocks would involve either poly-baric melting of an isotopically heterogeneous mantle source or contamination by lower crustal rocks such as proposed for Iceland alkaline magmas by Steinthorsson and others (1985). Magmatic suites that show a transition from alkaline to subalkaline basalt composition, such as those exposed in Hawaii and Iceland, commonly show a volume and time relationship to alkalinity, with small-volume extrusive sequences (typically formed early or late in the magmatic history) being alkaline and the large-volume phase of volcanism being subalkaline (Steinthorsson and others, 1985; Moore and others, 1982; Staudigel and others, 1984). Steinthorsson and others (1985) proposed an alternative to traditional mantle-melting models (poly-baric and/or metasomatic) for oceanic alkali basalts in which alkaline magmas are derived from mixtures of a primary tholeiitic melt and a nepheline-normative lower crustal component derived from the breakdown of kaersutite. This is an appealing model because it accounts for the volume relationships; small magma batches would more easily be contaminated by crustal melts. Such a model could also be applied to Red Sea rift magmatism, and cannot at present be fully discounted, however, the following factors favor mantle-level control:

1) The flood basalts of Saudi Arabia and Jordan constitute a major (90,000 km^2) flood basalt province, characterized by large-volume fissure eruptions of relatively low $^{87}Sr/^{86}Sr$ (0.7033 to 0.7037 - Coleman and others, 1983) alkali olivine basalt. The basalts contain peridotite nodules that were rapidly transported from depths of about 60 km (Coleman and others, 1983; Ghent and others, 1980; Kuo and Essene, 1986), below the 40 km-thick Arabian Shield (Mooney and others, 1985). The most primitive lavas in the flood basalt fields are picrites that cluster near the 2 GPa invariant in projections of the basalt system (Coleman and others, 1983; fig. 9). The flood basalts overlap in age with rift magmatism and demonstrate a mantle source for alkali basalt in the region during rifting.

2) A key element in the Iceland alkaline magmas is a systematic difference in $^{87}Sr/^{86}Sr$ relative to less radiogenic tholeiitic basalts (Steinthorsson, 1985). Although the isotopic data set from Red Sea rift rocks is limited, no systematic differences are observed between alkaline and subalkaline early rift magmas from the Al Lith region. In addition, the lowest initial Sr ratio is 0.7031 from hawaiite (table 1). However, Red Sea axial tholeiites have distinctly lower $^{87}Sr/^{86}Sr$ of 0.7026-0.7027 (Coleman and others, 1983).

3) As shown in ophiolite and MORB studies (Stolper, 1980; Pallister and Gregory, 1983), a poly-baric model is also capable of explaining volume-alkalinity relations, including the transition from small-volume rift eruptions of mixed affinity to large-volume tholeiitic Red Sea axis magmatism (see below).

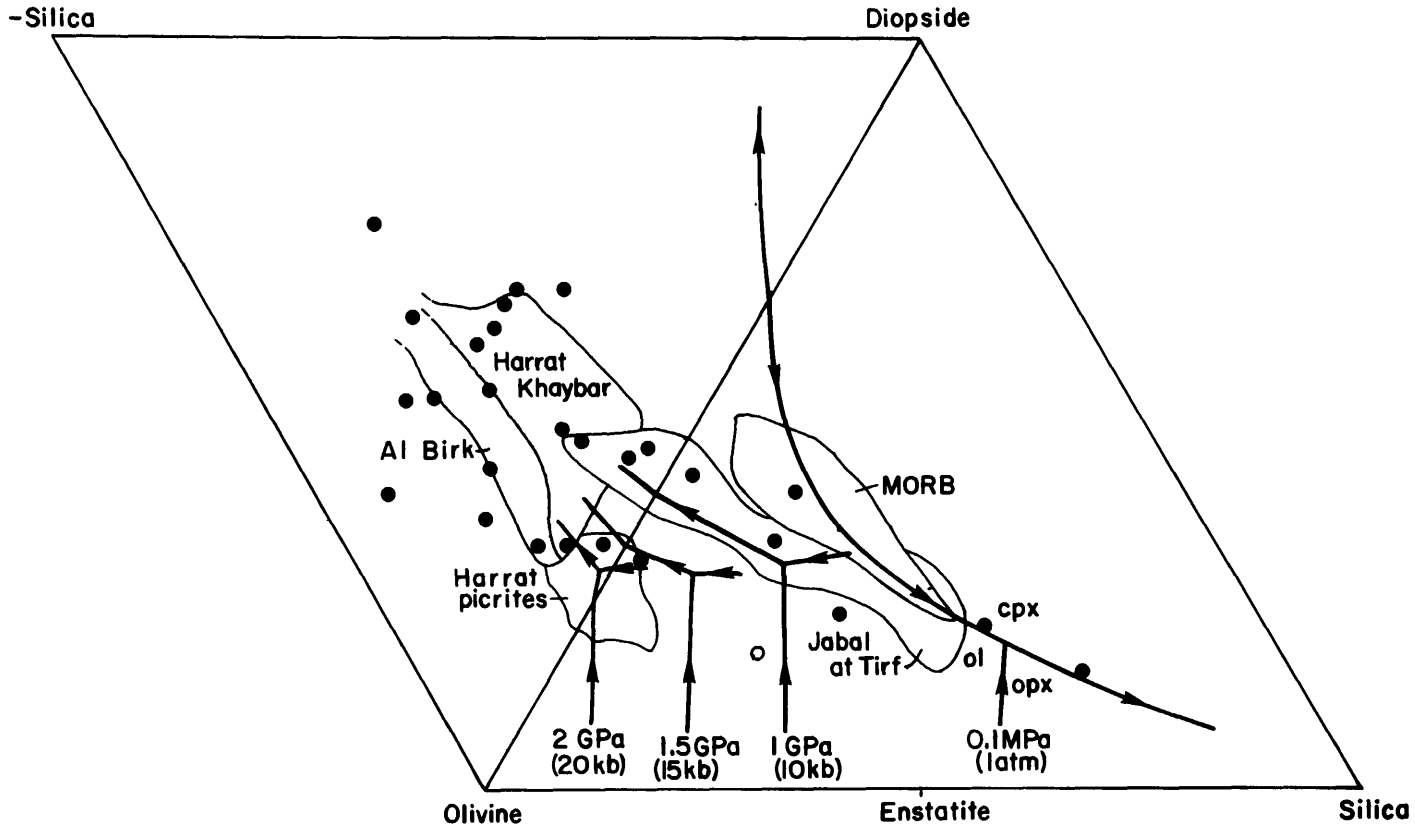

Figure 9.--*Liquids phase relations for basaltic melts from Stolper (1980) and Walker and others (1979) projected from plagioclase onto the diopside-olivine-silica surface of the simplified basalt phase system using the method of Walker and others (1979) except that undersaturated rocks are projected in an adjacent ternary in which -Silica expresses the degree of silica undersaturation (-Silica is plotted rather than nepheline to allow direct comparison with the experimentally determined boundaries). Arrowheads indicate decreasing temperatures on cotectics. Symbols as follow: ol=olivine, cpx=clinopyroxene, opx=orthopyroxene. Chemical data for mafic igneous rocks of the Al Lith region and fields for Cenozoic alkali flood basalts (Harrat Khaybar, Al Birk, and Harrat picrites) and a field for the Tertiary Jabal at Tirf complex from Coleman and others (1983) are shown. Solid dots represent tholeiites, alkali basalts, hawaiites, and one diorite (andesite chemistry), the open circle is a high-MgO tholeiite (175834).*

It has long been recognized that the invariant point in the basalt system crosses the plane of silica saturation (represented by the diopside-olivine join in figure 9) with increasing pressure (O'Hara, 1968). This relationship has been used to explain transitions from alkaline to subalkaline magmatism in various settings (e.g., Malpas, 1978) and can also be used to explain production of both types of melts in the Red Sea rift. Invariant melting of lherzolitic mantle at $\geq$2 GPa produces alkaline melts, lower-pressure melting (e.g. 1.5 GPa) produces subalkaline melts (fig. 9). Efficient melt transport, without reequilibration during ascent through the mantle, would result in the extrusion of both types at the surface as early rift lavas. Variable amounts of reequilibration and high-pressure (>0.5 GPa) fractionation of large- and small-volume melt batches during ascent through the upper mantle would also explain mixed affinity basalts during the early rift stage. This early period of mixed affinity magmatism would then be followed by deep production of Harrat alkaline basalts under the Arabian Shield and shallow production of the voluminous subalkaline mid-ocean ridge basalts of the axial region of the Red Sea from a more depleted mantle source.

Coleman and others (1983) explained Harrat basalt petrogenesis in terms of primary melting at pressures in excess of 2 GPa (20 kb) followed by high-pressure (>1 GPa) mantle fractionation, based on the "fanning" of Harrat volcanic compositions through the silica undersaturated region of figure 9. The distribution of alkali basalt and hawaiite compositions for the Harrat Khaybar and Al Birk flood basalt fields (fig. 9) was cited by Coleman and others as evidence for derivation of the Khaybar lavas at <40 kilometers depth (<1.5 GPa) and of the Al Birk lavas at >40 kilometers depth (>1.5 GPa).

Projections of the major element compositions of mafic rift volcanics and hypabyssal rocks from the Lith region overlap the entire range of the Harrat lavas and extend across the silica-saturated field to the low-pressure cotectic in figure 9. This wide range is interpreted to be the result of primary melting at about 60-70 kilometers (about 2 GPa) followed by poly-baric mantle-level cotectic olivine-clinopyroxene fractionation, and minor shallow-level crystal fractionation.

GEOLOGIC AND IGNEOUS HISTORY

Schematic paleogeographic reconstructions of the coastal plain in the Al Lith quadrangle are shown in figure 10. A horst-graben model explains the geology most simply and is adopted here. Tilted block faulting or listric faulting models are also applied to continental rifts (Cape and others, 1983) and listric or detachment faults are recognized in several areas of the Saudi Arabian coastal plain (Fairer, 1986, Bohannon, 1986 b unpub. data). Although structural data are only available from reconnaissance geologic mapping, attitudes in the Proterozoic rocks on each side of the Sita graben do not show rotation consistent with listric faulting.

Initial volcanism in figure 10 is shown beginning during the Eocene (about 50 Ma), when there was deposition of near-sea-level laterite and the upper Shumaysi formation. Coleman (1984a) points out that marine transgressions from the ancestral Mediterranean reached south of Jiddah during Paleocene and Eocene Shumaysi deposition. By 45 Ma ago, magmatism was underway in the Damm dike complex and at Jabal Sita. At the same time, quartz arenite and oolitic ironstone interbeds of the Shumaysi formation were being deposited from detritus shed into the incipient Sita graben from saprolite and laterite capping adjacent horst blocks. The elevation of the horst blocks probably did not exceed the thickness of

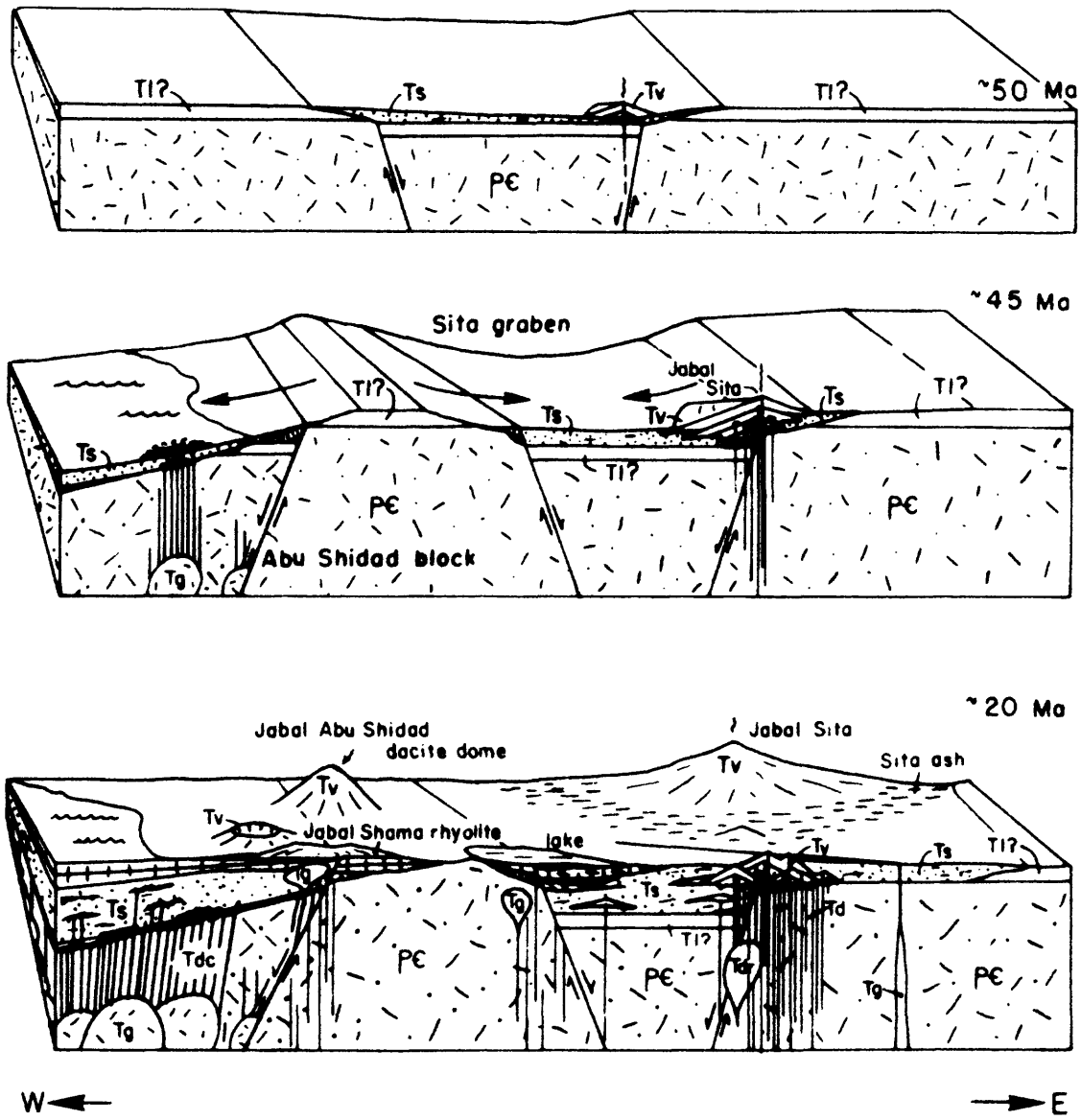

Figure 10.--*Schematic paleogeographic reconstruction diagram of the coastal plain in the Al Lith quadrangle. p€, Precambrian rocks; Tl, laterite and weathered Precambrian rock; Ts, Shumaysi formation and younger Tertiary sedimentary rocks; Tv, Sita formation; Td, Damm dike complex; Tg, gabbro and monzogabbro (plutons and Gumayqah complex dikes) Tdc, sheeted mafic dike complex (of hypothetical Red Sea crust); Tdr, Burgatinah diorite. Relative thicknesses of individual units (especially Tl) are exaggerated for clarity.*

the saprolite developed on the Precambrian basement. This sequence of events resulted both in the interbedding of Sita volcanic and volcaniclastic rocks with the upper Shumaysi and in a volcanic-ash component in the upper Shumaysi sedimentary rocks.

Between 45 Ma and about 20 Ma ago, graben depression, sedimentation, and transitional alkaline to subalkaline bimodal volcanism continued. Dike intrusion continued, and small plutons were emplaced at shallow levels. At about 20 Ma ago, widespread thick gabbro and monzogabbro dikes of the Gumayqah complex were intruded along predominantly northwesterly trends. Intrusion of the Damm dike complex and Sita formation volcanism apparently ceased at this point. Only the alkali basalts at Harrat ad Damm (11 Ma) and at Harrat Tuffil (3 Ma) have been erupted subsequently in the coastal plain of the Al Lith region. At some time after about 20 Ma ago, organized spreading and formation of oceanic crust began west of the Abu Shidad block.

The change in style of intrusion at about 20 Ma from the dense dike swarms of the Damm complex to the widely spaced, thick, gabbro dikes of the Gumayqah complex indicates a change in the regional stress field, and it may correlate with a change in plate motions and initiation of spreading in the proto-Red Sea. Coleman and others (1983, p.74) note a somewhat later change from the northwesterly trends of late Oligocene to early Miocene dikes and intrusions (including Gumayqah correlative dikes) to northerly trends of early Miocene and later volcanic vent alignments. They relate the change to the beginning of left-lateral motion along the Dead Sea Rift and slight counterclockwise rotation of the Arabian Plate away from Africa.

The latest reconstruction in figure 10 is for a time about 20 Ma ago and corresponds to the close of the initial continental-rift valley stage of Schmidt and others (1982). Faulting has continued since 20 Ma ago, and the present structural setting is more complicated than that shown in figure 10. The post-20 Ma structural history may include significant continental extension by low-angle faulting. Bohannon (1986b) documents post-25 Ma continental extension by detachment faulting in the southern coastal plain as well as expansion brought about by dike-swarm intrusion. But, unlike the southern part of the Arabian coastal plain, where pre-Tertiary sedimentary rocks and erosion surfaces provide geometric constraints, much of the record is eroded or buried below Quaternary sediments.

COMPARISON WITH OTHER AREAS

Long (>30 Ma) histories of within-plate magmatism are not without precedent. The Cameroon volcanic line of west-central Africa has been active for the past 65 Ma (Norry and Fitton, 1983) and the Hawaiian-Emperor seamount chain records about 70 Ma of basaltic magmatism derived from a mantle "plume" (Basaltic Volcanism Study Project, 1981). Isotopic data from various oceanic islands, as well as incompatible-element data from alkali basalts erupted through continental and oceanic crust along the Cameroon Line show that many oceanic and continental alkali basalts have a common source below the lithosphere, within the convecting upper mantle (Norry and Fitton, 1983; Thompson, 1986).

Comparison of the history of Red Sea rift magmatism developed for the Saudi Arabian coastal plain to that of the East African rift reveals a number of

similarities. Periodic volcanism, beginning 50-60 Ma ago, is also documented in the East African rift. Early determinations of old (>30 Ma) dates from Ethiopia (Megrue and others, 1972) have been shown to be erroneous (Jones, 1976). However, more recent determinations (Davidson and Rex, 1980) indicate that volcanism in Ethiopia began 50-60 Ma ago, but the rift valley was not clearly in evidence until 15 Ma ago (Mohr, 1983). Similarly, there is an apparent lag between initial volcanism in the Arabian coastal plain ($\geq$50 Ma?) and evidence of major uplift and extension. Schmidt and others (1982) argue that a continental rift valley did not develop until between 30 and 20 Ma ago and uplift of the Arabian continental margin did not occur until 10-15 Ma ago. The apparent lag between initial volcanism and major extension within the Red Sea-East African rift system suggests an asthenospheric initiation of continental rifting, rather than magmatism being strictly a consequence of continental thinning as described by Le Pichon and Sibuet (1981).

Barberi and others (1980) describe subalkaline and transitional alkaline basalts and trachytes from the Afar depression of Ethiopia with initial $^{87}Sr/^{86}Sr$ ratios of from 0.7033-0.7041. They see no evidence of continental crustal contamination and argue that the variation in strontium isotopic ratios is the result of progressively tapping more depleted (less radiogenic) source regions within a vertically heterogeneous mantle during rifting and spreading. The REE abundances and Sr isotopic ratios of the Al Lith rocks are also similar to those in Kenyan alkali basalts, nephelinites, and trachytes and as well as to alkali basalts from oceanic islands in general (see summary by Norry and Fitton, 1983). The Kenyan lavas have $^{143}Nd/^{144}Nd$ ratios that range between about 0.5129 and 0.5126 and $^{87}Sr/^{86}Sr$ ratios between about 0.7032 and 0.7047 (Norry and others, 1980).

MANTLE UNDERFLOW?

The eastern margin of the Red Sea is marked by an escarpment that rises to 3700 m in Yemen and gradually decreases in relief to the north in Saudi Arabia (Coleman, 1984a). Uplift postdates early rift magmatism and is thought to have occurred in two stages: during the Miocene, and during and following the Pliocene (Schmidt and others, 1982). High relief (to 2637 m) is also evident in the Sinai where fission-track studies indicate that uplift began at about 27 Ma and totals at least 5 km, with 3 km of the uplift post-dating 9 Ma (Kohn and Eyal, 1981). Harrat volcanism has been mostly restricted to the eastern margin of the Red Sea; only a few small flood basalt fields occur in Egypt and the Sudan (UNESCO, 1963). These features suggest that uplift and volcanism are related to the migration of a mantle thermal anomaly under the Arabian plate.

The Tertiary igneous rocks of the Saudi Arabian coastal plain provide a fragmentary, but long-duration record of the magmatic history of Red Sea rift and paar formation. Volcanic rocks in Saudi Arabia more distant from the Red Sea and Dead Sea record progressively less of the history. This relationship is indicated by the distribution of post-100 Ma radiometric dates of volcanic rocks from Saudi Arabia when compared to distance from the Red Sea and Dead Sea (M. E. Gettings, written commun., 1983). Except for old (18-23 Ma) basalt stocks from north-central Saudi Arabia (Stoeser and Elliott, 1985; Kellogg, 1985), the age of initial volcanism at the Harrat basalt fields decreases toward the interior of the Arabian Shield.

Gettings (1984) interprets Tertiary uplift of the Arabian continental margin and tilting of the regional gravity field of the Arabian Shield as effects of lateral density differences in the asthenosphere brought about by progressive lateral mantle flow (thermal convection) below the Shield during sea-floor spreading. Steckler (1985) notes that lithospheric heating due to extension is also insufficient to explain uplift bordering the Gulf of Suez and calls for secondary mantle convection induced by rifting to explain uplift by heating of the lithosphere adjacent to the rift.

Migration of an asthenospheric melting anomaly toward the interior of the Arabian plate (and to greater depth) may also explain the transition from combined alkaline and subalkaline magmatism during rifting to picritic and alkali basalt magmatism at the Harrat flood basalt fields. Although rift volcanism apparently began at about 50 Ma, lateral mantle flow and major crustal extension below Arabia was not well established until after 30 Ma.

ACKNOWLEDGMENTS

This study was aided by discussions with D. L. Schmidt, R. T. Gregory, R. G. Coleman, H. R. Blank, Jr., M. E. Gettings, K. S. Kellogg, R. G. Bohannon, and J. C. Cole. The manuscript was improved through critical reviews by D. L. Schmidt, R. G. Coleman, H. Stein, T. L. Wright, and an anonymous referee for the Geological Society of America Bulletin. Chemical analyses were performed by X-ray Assay Laboratories, Don Mills, Ontario, Canada and by the U.S. Geological Survey. K-Ar radiometric determinations were made by the Australian Mineral Development Laboratories (AMDEL), Eastwood, South Australia. The author thanks Alan Webb, Mark Fanning, and coworkers of AMDEL for their part in this study and for their conservative approach to commercial K-Ar work. The author would also like to thank C. W. Naeser for determining fission track ages. The work on which this report is based was conducted as part of a work agreement between the Saudi Arabian Directorate General of Mineral Resources and the U.S. Geological Survey.

DATA STORAGE

Data work and materials used in preparation of this report are archived as Data-File USGS-DF-05-4 stored in the office of the U. S. Geological Survey Mission in Jiddah, Saudi Arabia.

No updated information was added to the Mineral Occurrence Documentation System (MODS) data bank and no new localities were established in connection with this work.

REFERENCES CITED

Al-Shanti, A. M. S., 1966, Oolitic iron ore deposits in Wadi Fatimah between Jeddah and Mecca, Saudi Arabia: Saudi Arabian Directorate General of Mineral Resources Bulletin 2, 51 p.

ARGAS (Arabian Geophysical and Surveying Company), 1977, Geophysical synthesis report, eastern part of the central Red Sea, August 1977: Arabian Geophysical and Surveying Company (ARGAS) unnumbered report, 26 p.

Barberi, F., Civetta, L., and Varet J., 1980, Sr isotopic composition of Afar volcanics and its implications for mantle evolution: Earth and Planetary Science Letters, v. 50, p. 247-259.

Bartov, Y., Steinitz, G., Eyal, M., and Eyal, Y., 1980, Sinistral movement along the Gulf of Aqaba--Its age and relation to the opening of the Red Sea: Nature, v. 285, no. 5762, p. 220-221.

Basaltic Volcanism Study Project, 1981, Basaltic volcanism on the terrestrial planets: New York, Pergammon Press, 1286 p.

Blank, H. R., Jr., 1977, Aeromagnetic and geologic study of Tertiary dikes and related structures on the Arabian margin of the Red Sea: Saudi Arabian Directorate General of Mineral Resources Bulletin 22, p. G1-G18.

Blank, H. R., Jr., Mooney, W. D., Healy, J. H., Gettings, M. A., and Lamson, R. J., 1986, A seismic refraction interpretation of the eastern margin of the Red Sea: Saudi Arabian Deputy Ministry for Mineral Resources Open-File Report USGS-OF-05-23, 20 p. Also, 1986, U.S. Geological Survey Open-File Report 86-257.

Blank, H. R., Jr., Johnson, P. R., Gettings, M. E., and Simmons, G. C., 1986, Geologic map of the Jizan quadrangle, sheet 16F, Kingdom of Saudi Arabia, Saudi Arabian Directorate General of Mineral Resources Geoscience Map, GM-104-C, 1 plate, scale 1:250,000 [in press].

Brown, G. F., Jackson, R. O., Bogue, R. G., and MacLean, W. H., 1963, Geologic map of the southern Hijaz quadrangle, Kingdom of Saudi Arabia: U.S. Geological Survey Miscellaneous Geologic Investigations Map I-210-A, scale 1:500,000.

Cape, C. D., McGeary, S., and Thompson, G. A., 1983, Cenozoic normal faulting and shallow structures of the Rio Grande rift near Socorro, New Mexico: Geological Society of America Bulletin, v. 94, p. 3-14.

Chayes, F., 1970, Experimentation in the electronic storage and manipulation of large numbers of rock analyses: Carnegie Institute of Washington Yearbook, v. 68, p. 174-187.

Christensen, E. H., Bikun, J. V., Sheridan, M. F., and Burt, D. M., 1984, Geochemical evolution of topaz rhyolites from the Thomas Range and Spor Mountain, Utah: American Mineralogist, v. 69, p. 223-236.

Cochran, J. R., 1983, A model for the development of the Red Sea: American Association of Petroleum Geologists Bulletin, v. 67, p.41-69.

Coleman, R. G., 1974, Geologic background of the Red Sea: Initial Reports of the Deep Sea Drilling Project, v. 23, p. 813-819.

_____ 1984a, The Red Sea: A small ocean basin formed by continental extension and sea floor spreading in Proceedings, International Geological Congress, 27th, Moscow: Utrecht, The Netherlands, v. 23, p. 93-121.

_____ 1984b, The Tihamat Asir igneous complex, a passive margin ophiolite in Proceedings, International Geological Congress, 27th, Moscow: Utrecht, The Netherlands, v. 9, p. 221-239.

Coleman, R. G., Fleck, R. J., Hedge, C. E., and Ghent, E. D., 1977, The volcanic rocks of southwest Saudi Arabia and the opening of the Red Sea: Saudi Arabian Directorate General of Mineral Resources Bulletin 22, p. D1-D30.

Coleman, R. G., Gregory, R. T., and Brown, G. F., 1983, Cenozoic volcanic rocks of Saudi Arabia: Saudi Arabian Deputy Ministry for Mineral Resources Open-File Report USGS-OF-03-93 (Interagency Report 594), 82 p. Also, 1983, U.S. Geological Survey Open-File Report 83-788.

Davidson, A., and Rex, D. C., 1980, Age of volcanism and rifting in southwestern Ethiopia: Nature, v. 283, p. 657-658.

Fairer, G. M., 1986, Geology of the Wadi Baysh quadrangle, sheet 17F, Kingdom of Saudi Arabia: Saudi Arabian Deputy Ministry for Mineral Resources Geoscience Map GM-77, scale 1:250,000 [in press].

Faure, G., and Powell, J. L., 1972, Strontium isotope geology: New York, Springer-Verlag, 188 p.

Fitch, F. H., 1980, Saudi Arabian stratigraphic lexicon: Saudi Arabian Deputy Ministry for Mineral Resources Technical Record DM-01-1, 273 pp.

Fleck, R. J., and Hadley, D. G., 1982, Ages and strontium initial ratios of Plutonic rocks in a transect of the Arabian Shield: Saudi Arabian Deputy Ministry for Mineral Resources Open-File Report USGS-OF-03-38 (Interagency Report 535), 43 p. Also, 1985, U.S. Geological Survey Open-File Report 85-727.

Gast, P. W., 1968, Trace element fractionation and the origin of tholeiitic and alkaline magma types: Geochimica et Cosmochimica Acta, v. 32, p. 1057-1086.

Gettings, M. E., 1977, Delineation of the continental margin in the southern Red Sea region from new gravity evidence, in Red Sea research, 1970-75: Saudi Arabian Directorate General of Mineral Resources Bulletin 22, p. K1-K11.

Gettings, M. E., 1983, A simple Bouguer gravity map of southwestern Saudi Arabia and an initial interpretation: Saudi Arabian Deputy Ministry for Mineral Resources Open-File Report USGS-OF-03-94 (Interagency Report 595), 89 p. Also, 1983, U.S. Geological Survey Open-File Report 83-789.

_____ 1984, The isostatic gravity anomaly field of southwestern Saudi Arabia and its interpretation: Saudi Arabian Deputy Ministry for Mineral Resources Technical Record USGS-TR-04-22 (Interagency Report 696), 107 p., 3 pl. Also, 1985, U.S. Geological Survey Open-File Report 85-254.

Gettings, M. E., and Stoeser, D. G., 1981, A tabulation of radiometric age determinations for the Kingdom of Saudi Arabia: U.S. Geological Survey Saudi Arabian Mission Miscellaneous Document 20 (Interagency Report 353), 52 p.

Gettings. M. E., Blank, H. R., Mooney, W. D., and Healey, J. H., 1983, Crustal structure of southwestern Saudi Arabia: Saudi Arabian Deputy Ministry for Mineral Resources Open-File Report USGS-OF-03-59 (Interagency Report 560), 51 p. Also, 1981, U.S. Geological Survey Open-File Report 81-800.

Ghent, E. D., Coleman, R. G., and Hadley, D. G., 1980, Ultramafic inclusions and host alkali olivine basalts of the southern coastal plain of the Red Sea, Saudi Arabia: American Journal of Science, v. 280-A, p. 499-527.

Green, T. H., and Pearson, N. J., 1985, Experimental determination of REE partition coefficients between amphibole and basaltic to andesitic liquids at high pressure: Geochimica et Cosmochimica Acta, v. 49, p. 1465-1468.

Grolier, M. J., and Overstreet, W. C., 1978, Geologic map of Yemen Arab Republic (San'a): U.S. Geological Survey Miscellaneous Investigations Series, Map I-1143-B, Scale 1:500,000.

Hadley, D. G., and Fleck, R. J., 1980, Reconnaissance geologic map of the Al Lith quadrangle, sheet 20/40 C, Kingdom of Saudi Arabia: Saudi Arabian Directorate General of Mineral Resources Geologic Map GM-32, 10 p., 1 sheet, scale 1:100,000.

Hildreth, Wes, 1979, The Bishop Tuff: Evidence for the origin of compositional zonation in silicic magma chambers: Geological Society of America Bulletin Special paper 180, p. 43-75.

Henderson, P., 1984, General geochemical properties and abundances of the rare earth elements in Henderson, P., ed., Rare Earth Element Geochemistry: Elsevier, Amsterdam, p. 1-32.

Huang, W. L., and Wyllie, P. J., 1981, Phase relationships of S-type granite with H_2O to 35 kbar: Muscovite granite from Harney Peak, South Dakota: Journal of Geophysical Research, v. 86, p. 10515-10529.

Irvine, T. N., and Baragar, W. R. A., 1971, A guide to the chemical classification of the common volcanic rocks: Canadian Journal of Earth Sciences, v. 8, p. 523-548.

Irving, A. J., 1978, A review of experimental studies of crystal/liquid trace element partitioning: Geochimica et Cosmochimica Acta, v. 42, p. 743-770.

Irving, A. J., and Frey, F. A., 1978, Distribution of trace elements between garnet megacrysts and host volcanic liquids of kimberlitic to rhyolitic composition: Geochimica et Cosmochimica Acta, v. 42, p. 771-787.

Irving, A. J., and Frey, F. A., 1984, Trace element abundances in megacrysts and their host basalts: Constraints on partition coefficients and megacryst genesis: Geochimica et Cosmochimica Acta, v. 48, p. 1201-1221.

Jones, P. W., 1976, Age of the lower flood basalts of the Ethiopian plateau: Nature, v. 261, p. 567-569.

Keesman, I., Matthes, S., Schreyer, W., and Seifert, F., 1971, Stability of almandine in the system $FeO-(Fe_2O_3)-Al_2O_3-SiO_2-(H_2O)$ at elevated pressures: Contributions to Mineralogy and Petrology, v. 31, p. 132-144.

Kohn, B. P., and Eyal, M., 1981, History of uplift of the crystalline basement of Sinai and its relation to opening of the Red Sea as revealed by fission track dating of apatites: Earth and Planetary Science Letters, v. 52, p. 129-141.

Karpoff, R., 1957a, Sur l'existence du Maestrichtien au nord de Djeddah (Arabie Seoudite): Comptes Rendus Hebdomadaires des Sciences, v. 245, no. 16, p. 1322-1324.

_____ 1957b, Esquisse geologique de l'Arabie Seoudite: Bulletin de las Societe Geologique de France, ser. 6, v. 7, no. 6, p. 653-696.

Kellogg, K. S., 1985, Reconnaissance geology of the Qufar quadrangle, sheet 27/41D, Kingdom of Saudi Arabia: Saudi Arabian Deputy Ministry for Mineral Resources Open-File Report USGS-OF-04-2 (Interagency Report 626), 35 p, 2 sheets, scale 1:100,000. Also, 1984, U.S. Geological Survey Open-File Report 84-159.

Kuo, L-C, and Essene, E. J., 1986, Petrology of spinel harzburgites from the al Kishb Plateau, Saudi Arabia: Implications on the Thermal History of the upper mantle beneath the Arabian Shield: Contributions to Mineralogy and Petrology [in press].

Le Pichon, Xavier, and Sibuet, Jean-Claude, 1978, Passive Margins: A model of formation: Journal of Geophysical Research, v. 86, p. 3708-3720.

Madden, C. T., 1983, Paleocene pycnodont fishes from Jabal Umm Himar, Harrat Hadan area, Kingdom of Saudi Arabia, U.S. Geological Survey Open-File Report 83-453, 25 p.

Madden, C. T., Naqvi, I. M., Whitmore, F. C., Jr., Schmidt, D. L., Langston, W., Jr., and Wood, R. C., 1979, Paleocene vertebrates from coastal deposits in the Harrat Hadan area, At Taif region, Kingdom of Saudi Arabia: U.S. Geological Survey Open-File Report 80-227, 29 p.

Mahood, Gail, and Hildreth, Wes, 1983, Large partition coefficients for trace elements in high-silica rhyolites: Geochimica et Cosmochimica Acta, v. 47, p. 11-30.

Malpas, J., 1978, Magma generation in the upper mantle, field evidence from ophiolite suites, and applications to the generation of oceanic lithosphere: Philosophical Transactions, Royal Society of London, Ser.A, v. 288, p.527-546.

Megrue, G. H., Norton, E., and Strangway, D. W., 1972, Tectonic history of the Ethiopian rift as deduced by K-Ar ages and paleomagnetic measurements of basaltic dikes: Journal of Geophysical Research, v. 77, p. 5744-5754.

Mohr, P., 1983, Volcanotectonic aspects of Ethiopian rift evolution: Bulletin des Centres de Recherches Exploration-Production Elf-Aquitaine, v. 7, p. 175-189.

Moltzer, J. G., and Binda, P. L., 1981, Micropaleontology of the middle and upper members of the Shumaysi formation, Saudi Arabia: Bulletin of the Faculty of Earth Sciences, King Abdulaziz University, Jiddah, Saudi Arabia, v. 4, p. 57-76.

Mooney, W. D., Gettings, M. E., Blank, H. R., and Healy, J. H., 1985, Saudi Arabian seismic-refraction profile: A traveltime interpretation of crustal and upper mantle structure: Tectonophysics, v.111, p. 173-246.

Moore, J. G., Clague, D. A., and Normark, W. R., 1982, Diverse basalt types from Loihi seamount, Hawaii: Geology, v. 10, p. 88-92.

Nagasawa, H., 1970, Rare earth concentrations in zircons and apatites and their host dacites and granites: Earth and Planetary Science Letters, v. 9, p. 359-364.

Norry, M. J., Truckle, P. H., Lippard, S. J., Hawkesworth, C. J., Weaver, S. D., and Marriner, G. F., 1980, Isotopic and trace element evidence from lavas, bearing on mantle heterogeneity beneath Kenya: Philosophical Transactions of the Royal Society of London, series A, v. 297, p. 259-271.

Norry, M. J., and Fitton, J. G., 1983, Compositional differences between oceanic and continental basic lavas and their significance in Hawkesworth, C. J., and Norry, M. J., eds., Continental Basalts and Mantle Xenoliths: Shiva Publishing, Ltd., Cheshire, U. K., p. 5-19.

O'Hara, M. J., 1968, The bearing of phase equilibria studies on the origin and evolution of basic and ultrabasic rocks, Earth Science Reviews, v. 4, p. 69-133.

Padovani, E. R., and Carter, J. L., 1981, Non-equilibrium partial fusion due to decompression and thermal effects in crustal xenoliths in Dick, H. J. B., ed., Magma Genesis: Oregon Department of Geology and Mineral Industries Bulletin 96, p. 43-56.

_____ 1982c, Reconnaissance geologic map of the Harrat Tuffil quadrangle, sheet 20/39 B, Kingdom of Saudi Arabia: Saudi Arabian Deputy Ministry for Mineral Resources Open-File Report USGS-OF-03-33 (Interagency Report 530), 2 sheets, scale 1:100,000. Also, 1983, U.S. Geological Survey Open-File Report 83-332.

Pallister, J. S., 1986, Explanatory notes to the geologic map of the Al Lith quadrangle, sheet 20D, Kingdom of Saudi Arabia: Saudi Arabian Directorate General of Mineral Resources Geoscience Map GM-95, 143 p., scale 1:250,000 [in press].

Pallister, J. S., and Gregory, 1983, Composition of the Samail ocean crust: Geology, v. 11, p. 638-642.

Powers, R. W., Ramirez, L. F., Redmond, C. D., and Elberg, E. L., Jr., 1966, Geology of Saudi Arabia: U. S. Geological Survey Professional Paper 560-D, 147 p.

Riofinex Geological Mission, 1980, Airborne magnetometer-scintillation counter survey of the Kingdom of Saudi Arabia, Al Lith quadrangle, sheet 20D, 1:250,000-scale; unpublished regional report.

Schmidt, D. L., Hadley, D. G., and Brown, G. F., 1982, Middle Tertiary continental rift and evolution of the Red Sea in southwestern Saudi Arabia: Saudi Arabian Deputy Ministry for Mineral Resources Open-File Report USGS-OF-03-6 (Interagency Report 503), 56 p. Also, 1983, U.S. Geological Survey Open-File Report 83-641.

Staudigel, H., Zindler, A., Hart, S. R., Leslie, T., Chen, C.-Y., and Clague, D., 1984, The isotopic systematics of a juvenile intraplate volcano: Pb, Nd, and Sr isotope ratios of basalts from Loihi Seamount, Hawaii: Earth and Planetary Science Letters, v. 69, p. 13-29.

Steckler, M. S., 1985, Uplift and extension at the Gulf of Suez - Indications of induced mantle convection: Nature, v. 317, p. 135-139.

Steinthorsson, Sigurdur, Osakarsson, Niels, and Sigvaldason, G. E., 1985, Origin of alkali basalts in Iceland: A plate tectonic model: Journal of Geophysical Research, v. 90, p. 10027-10042.

Stern, C. R., and Wyllie, P. J., 1981, Phase relationships of I-type granite with H_2O to 35 kilobars: The Dinkey Lakes biotite-granite from the Sierra Nevada batholith: Journal of Geophysical Research, v. 86, p. 10412-10422.

Stoeser, D. B., and Elliott, J. E., 1985, Reconnaissance geology of the Al Qasr quadrangle, sheet 27/41C, Kingdom of Saudi Arabia: Saudi Arabian Deputy Ministry for Mineral Resources Open-File Report USGS OF-05-2 (Interagency Report 707), 51 p. Also, 1985, U.S. Geological Survey Open-File Report 85-668.

Stolper, E., 1980, A phase diagram for mid-ocean basalts: Preliminary results and implications for Petrogenesis: Contributions to Mineralogy and Petrology, v.74, p.13-27.

Thompson, R. N., 1986, Sources of basic magmas: Nature, v. 319, p. 448-449.

UNESCO (United Nations Educational, Scientific and Cultural Organisation), 1963, Geological Map of Africa: UNESCO, Paris, scale 1:5,000,000, 9 pl.

Walker, D., Shibata, T., and Delong, S. E., 1979, Abyssal tholeiites from the Oceanographer Fracture Zone; II: Phase equilibria and mixing: Contributions to Mineralogy and Petrology, v.70, p. 111-125.

Watson, E. B., 1980, Some experimentally determined zircon/liquid partition coefficients for the rara earth elements: Geochemica et Cosmochimica Acta, v. 44, p. 895-897.

Wier, K. L., and Hadley, D. G., 1975, Reconnaissance geology of the Wadi Sa'diyah quadrangle, sheet 20/40 A, Kingdom of Saudi Arabia: U.S. Geological Survey Open-File Report 75-493, 27 p., scale 1:100,000.